Electronic Supplementary Material (ESI) for Dalton Transactions.

Electronic Supporting Information

for

Spin state variability in Fe^{2+} complexes of substituted (2-(pyridin-2-yl)-1,10-phenanthroline) ligands as versatile terpyridine analogues

Holm Petzold*[a)], Paul Djomgoue[a)], Gerald Hörner[b)], Silvio Heider[a)], Charles Lochenie[c)], Birgit Weber[d)], Tobias Rüffer[a)], and Dieter Schaarschmidt[a)]

a) TU Chemnitz, Institut für Chemie, Anorganische Chemie, Straße der Nationen 62, 09111 Chemnitz, Germany; Fax: +49-371-53137463; E-mail: holm.petzold@chemie.tu-chemnitz.de

b) TU Berlin, Institut für Chemie, Straße des 17. Juni 135, 10623 Berlin, Germany

c) Institut de science et d'ingénierie supramoléculaires (ISIS), Université de Strasbourg & CNRS, 8 Rue Gaspard Monge, 67000 Strasbourg, France

d) Anorganische Chemie II, Universität Bayreuth, Universitätsstraße 30, NWI, 95440 Bayreuth, Germany

1 ESI Content

1.1 Preparation of compounds

Syntheses of ligands

All ligands **5a-e** were prepared according to general literature protocols.[1,2] The compound **5a,5c** and **5d** were characterized by the published ^{1}H NMR data.[1,3–5]The compound **5b** was only obtained as an oily substance difficult to purify and was therefore used as received for synthesis of [Fe(**5b**)$_2$](BF$_4$)$_2$. Additional purification by complexation and decomplexation with [Zn(H$_2$O)$_6$](ClO$_4$)$_2$ afforded analytical grade **5b**.

2-(3-methoxypyridin-2-yl)-1,10-phenanthroline (**5b**) oil used as received: **^{1}H NMR** (500 MHz, CDCl$_3$) δ 9.10 (d, J = 5 Hz, 1H), 8.34 (d, J = 4.5 Hz, 1H), 8.21 (d, J = 8.5 Hz, 1H), 8.12 (d, J = 7.7 Hz, 1H), 8.03 (d, J = 8.5 Hz, 1H), 7.71 (d, J = 8.5 Hz, 1H), 7.68 (d, J = 8.2 Hz, 1H), 7.49 (dd, J = 8.2, 4.5 Hz, 1H), 7.28 (d, J = 8.2 Hz, 1H), 7.24 (dd, J = 8.2, 4.5 Hz, 1H), 5.19 (s, 3H, OCH_3); Anal. calcd. for $C_{18}H_{13}N_3O$ (287.32 g mol^{-1}): C 75.25, H 4.56, N 14.63; found: C 75.68, H 4.97, N 14.32.

2-(6-methoxypyridin-2-yl)-1,10-phenanthroline (**5c**) (white solid, 74%): Anal. calcd. for $C_{18}H_{13}N_3O$ (287.32 g mol^{-1}): C 75.25, H 4.56, N 14.63; found: C 75.10, H 5.12, N 13.42; **^{1}H NMR** (500 MHz, CDCl$_3$) δ 9.25 (dd, J = 4.3, 1.7 Hz, 1H), 8.81 (d, J = 8.4 Hz, 1H), 8.64 (dd, J = 7.4, 0.7 Hz, 1H), 8.34 (d, J = 8.4 Hz, 1H), 8.26 (dd, J = 8.0, 1.7 Hz, 1H), 7.80 (m, 3H), 7.64 (dd, J = 8.0, 4.4 Hz, 1H), 6.84 (dd, J = 8.2, 0.7 Hz, 1H), 4.11 (s, 3H, OCH_3); **^{13}C NMR** (125.80 MHz, CDCl$_3$) δ 163.51, 156.30, 153.34, 150.35, 146.32, 145.62, 139.54, 136.75, 136.26, 129.05, 128.72, 126.61, 126.56, 122.89, 120.87, 115.68, 111.54, 53.29 ppm (OCH$_3$). **ESI-MS** (CH$_2$Cl$_2$/acn): *m/z* calcd. for (**5c**+H)$^+$: 288.1131 found 288.1119 calced for (**5c**+Na)$^+$: 310.0951 found 310.0941.

2-(6-(1H-pyrazol-1-yl)pyridin-2-yl)-1,10-phenanthroline (**5e**) (yellow solid): Anal. calcd. for $C_{20}H_{13}N_5$ (323.35 g mol-1): C 74.29, H 4.05, N 21.66; found: C 73.98, H 3.99, N 21.55; **^{1}H NMR** (500 MHz, CDCl$_3$) δ 9.19 (dd, J = 4.3, 1.7 Hz, 1H), 8.85 (dd, J = 7.4, 1.1 Hz, 1H), 8.78 (d, J = 8.4 Hz, 1H), 8.73 (dd, J = 2.5, 1.7 Hz, 1H), 8.32 (d, J = 8.4 Hz, 1H), 8.20 (dd, J = 8.0, 1.7 Hz, 1H), 8.02 – 8.00 (dd, J = 2.5Hz, 1H), 8.00 – 7.97 (t, J = 7.4 Hz, 1H), 7.77 (m, 2H), 7.71 (d, J = 7.4, 1.1 Hz, 1H), 7.59 (dd, J = 8.0, 4.3 Hz, 1H), 6.45 (dd, J = 2.5, 1.7 Hz, 1H); **^{13}C NMR** (125.80 MHz, CDCl$_3$) δ: 155.3, 154.5, 150.9, 150.5, 146.2, 145.6, 142.0, 139.8, 137.0, 136.3, 129.1, 128.9, 126.5, 123.1, 120.8, 120.6, 112.8, 107.7, 104.6; **ESI-MS** (CH$_2$Cl$_2$/acn): *m/z* calcd. for (**5e**+H)$^+$: 324.1244 found 324.1286.

Synthesis of complexes

General procedure: A clear solution of 1 mmol of [Fe(H$_2$O)$_6$](BF$_4$/ClO$_4$)$_2$ in ethanol (50 mL) was added dropwise to a clear solution of ligand **5** (2 mmol) in ethanol/dichloromethane (1:5, 100 mL). The desired complexes [Fe($\mathbf{5}$)$_2$](BF_4/ClO_4) precipitate from the reaction mixture. The precipitation can be aided by the reduction of the solvent to 30% of the original volume and the addition of diethyl ether. The complexes were further purified by slow diffusion of diethyl ether to an acetonitrile solution of the complexes.

[Fe(**5a**)$_2$](BF_4)$_2$: Anal. calcd. for $C_{34}H_{22}B_2F_8FeN_6{\cdot}CH_3CN$ (%) C: 55.07, H: 3.21, N: 12.49 found. C: 54.76, H: 3.54, N: 12.86; **^{1}H NMR** (500 MHz, d_3-acetonitrile) δ 9.26 (m, 4H), 8.66 (d, J =7.9 Hz, 2H), 8.61 (d, J=9.0Hz, 2H), 8.35 (dd, J = 7.9, 1.3Hz, 2H) 8.30 (d, J = 9.0Hz, 2H), 7.91 (td, J =7.8, 1.4 Hz, 2H), 7.21 (m, 2H), 7.09 (d, J= 5.3 Hz, 2H), 6.97 (ddd, J = 7.1, 5.6, 1.2Hz, 2H). **ESI-MS** (CH_2Cl_2/acn): *m/z* calcd. for [Fe(**5a**)$_2$]$^{2+}$: 285.0622 found 285.0685;

[Fe(**5b**)$_2$](ClO_4)$_2$: Anal. calcd. for $C_{36}H_{26}Cl_2FeN_6O_{10}{\cdot}½H_2O$ (%) C: 51.57, H: 3.25, N: 10.02 found. C: 51.42, H: 3.22, N: 10.30; **^{1}H NMR** (500 MHz, d_6-acetone) δ 9.62 (d, J = 8.9 Hz, 2H, *H*7, T_1 = 2.8 sec), 9.18 (d, J = 8.9 Hz, 2H, *H*6, T_1 = 2.2 sec), 8.58 (d, J = 8.7 Hz, 2H, *H*5, T_1 = 2.1 sec), 8.34 (d, J = 7.9 Hz, 2H, *H*3, T_1 = 2.3 sec), 8.26 (d, J = 8.7Hz, 1.8 Hz, 2H, *H*4, T_1 = 2.0 sec), 7.53 (d, J = 8.7 Hz, 2H, *H*9, T_1 = 1.8 sec), 7.21 (dd, J = 8.7 Hz, J = 5.5 Hz, 2H, *H*2, T_1 = 2.1 sec), 7.13 (d, J = 5.5 Hz, 2H, *H*1, T_1 = 2.7 sec), 6.92 (dd, J = 8.7 Hz, J = 5.5 Hz, 2H, *H*10, T_1 = 2.0 sec), 6.96 (d, J = 5.5 Hz, 2H, *H*11, T_1 = 3.0 sec), 4.21 (s, 6H, OMe, T_1 = 1.0 sec). **ESI-MS** (CH_2Cl_2/acn): *m/z* calcd. for [Fe(**5b**)$_2$]$^{2+}$: 729.0953 found 729.0947;

[Fe(**5c**)$_2$](BF_4)$_2$: Anal. calcd. for $C_{36}H_{26}B_2F_8FeN_6O_2{\cdot}2(H_2O)$ (%) C: 51.47, H: 3.60, N 10.00: found. C: 51.76, H: 3.58, N: 9.66; **^{1}H NMR** (500 MHz, d_6-acetone) δ 39.2 (2H, *H*1), 22.93 (2H, *H*7, T_1 = 77 ms), 19.25 (2H, *H*8, T_1 = 89 ms), 17.93 (2H, *H*10, T_1 = 94 ms), 15.65 (2H, *H*2, T_1 = 109 ms), 11.29 (2H, H4, T_1 = 320 ms), 11.06 (2H, H3, T_1 = 250 ms), 10.09 (2H, H5, T_1 = 300 ms), 8.79 (2H, *H*9, T_1 = 250 ms), 4.68 (2H, *H*6, T_1 = 180 ms), 2.29 (6H, OMe, T_1 = 70 ms). **ESI-MS** (CH_2Cl_2/acn): *m/z* calcd. for [Fe(**5c**)$_2$]$^{2+}$: 315.0728 found 315.0739;

[Fe(**5d**)$_2$](BF_4)$_2$: Anal. calcd. for $C_{34}H_{20}B_2Br_2F_8FeN_6{\cdot}CH_3CN$ (%) C: 45.86, H: 2.46, N 10.40: found. C: 45.89, H: 2.64, N: 10.20, **^{1}H NMR** (500 MHz, d_6-acetone) δ 198 (2H, *H*1), 91.73 (2H, *H*7, T_1 = 12 ms), 63.55 (2H, *H*8, T_1 = 12 ms), 62.16 (2H, *H*10, T_1 = 15 ms), 57.54 (2H, *H*2, T_1 = 15 ms), 26.09 (2H, *H*4, T_1 = 57 ms), 22.24 (2H, *H*3, T_1 = 42 ms), 16.33 (2H, *H*5, T_1 = 51 ms), 15.56 (2H, *H*9, T_1 = 35 ms), -20.74 (2H, *H*6, T_1 = 27 ms); **ESI-MS** (CH_2Cl_2/acetonitrile): *m/z* calcd. for [Fe(**5d**)$_2$]$^{2+}$: 363.9719 found 363.9763;

[Fe(**5e**)$_2$](BF_4)$_2$: Anal. calcd. for $C_{40}H_{26}B_2F_8FeN_8{\cdot}1.5H_2O$ (%) C: 53.19, H: 3.24, N: 15.51: found. C: 53.22, H: 3.15, N: 15.33; **^{1}H NMR** (500 MHz, d_3-acetonitrile, 338 K) δ 110.9 (2H, T_1 = 0.13 ms), 62.19 (2H, T_1 = 2 ms), 52.34 (2H, T_1 = 2 ms), 51.09 (2H, T_1 = 0.3 ms), 43.20 (2H, T_1 = 2.7 ms), 41.61 (2H, T_1 = 3.5 ms), 36.38 (2H, T_1 = 3.8 ms), 30.31 (2H, T_1 = 2.9 ms), 21.30 (2H, T_1 = 9.5 ms), 20.03 (2H, T_1 = 10.8 ms), 19.71 (2H, T_1 = 8.2 ms), 11.27 (2H, T_1 = 5.3 ms), 11.04 (2H, T_1 = 5.6 ms); **ESI-MS** (CH_2Cl_2/acetonitrile): *m/z* calcd. for [Fe(**5e**)$_2$]$^{2+}$: 789.1694 found 789.1723;

[Zn(**5e**)$_2$](ClO_4)$_2$: Anal. calcd. for $C_{40}H_{26}Cl_2N_8O_8Zn{\cdot}3(CH_3CN)$ (%) C: 53.43, H: 3.41, N: 17.61: found. C: 53.39, H: 3.24, N: 17.42; **^{1}H NMR** (500 MHz, d_3-acetonitrile) δ 9.18 (d, J = 8.6 Hz, 2H, *H*6), 9.05 (d, J = 8.6 Hz, 2H, *H*7), 8.71 (d, J = 8.1 Hz, 2H, *H*5), 8.49 (dd, J = 7.2/2.0 Hz, 2H, *H*3), 8.38 (t, J = 8.1 Hz, 2H, *H*9), 8.31 (d, J = 9.2 Hz, 2H, *H*5), 8.17 (d, J = 9.0 Hz, 2H, *H*4), 7.62 (d, J = 8.0 Hz, 2H, *H*10), 7.56 (m, 2H, *H*1), 7.53 (m, 2H, *H*11), 7.47 (dd, J = 8.2/5.0 Hz, 2H, *H*2), 6.49 (bs, 2H, *H*13), 5.89 (bs, 2H, *H*12).

1.2 DFT-computational details

All DFT calculations were performed using ORCA2.9.1.[6] Large TZVPP basis sets[7] were used throughout. The structures of the cations [Fe(**5a-d**)$_2$]$^{2+}$ were optimized in their LS and HS states using five derivatives of the well-established hybrid functional B3LYP.[89] In these derivative functionals the amount of exact exchange a_0 has been varied stepwise from 0.20 (native B3LYP) to 0.00. The structure of the cation [Fe(**5e**)$_2$]$^{2+}$ was optimized in its LS and HS state with the amount of exact exchange a_0 fixed to 0.00. In this case, single-point energy calculations with $0.00 < a_0 \leq 0.20$ yielded the relative SCO energies. Cartesian coordinates of the B3LYP*-optimized structures (a_0 = 0.15) of [Fe(**5a-e**)$_2$]$^{2+}$ (*LS* and *HS*) are compiled in Table 16-SI to Table 25-SI and pertinent metrical features are given in Table 4-SI (optimization with a_0 = 0.00 for [Fe(**5e**)$_2$]$^{2+}$). The SCF energies were converged to 10^{-7} Hartree in energy. Dispersion contributions were approximated using Grimme's DFT-D6 atom-pairwise dispersion corrections of the parent B3LYP functional.[10] Numerical frequency calculations revealed the stationary points to be minima on the potential surface.

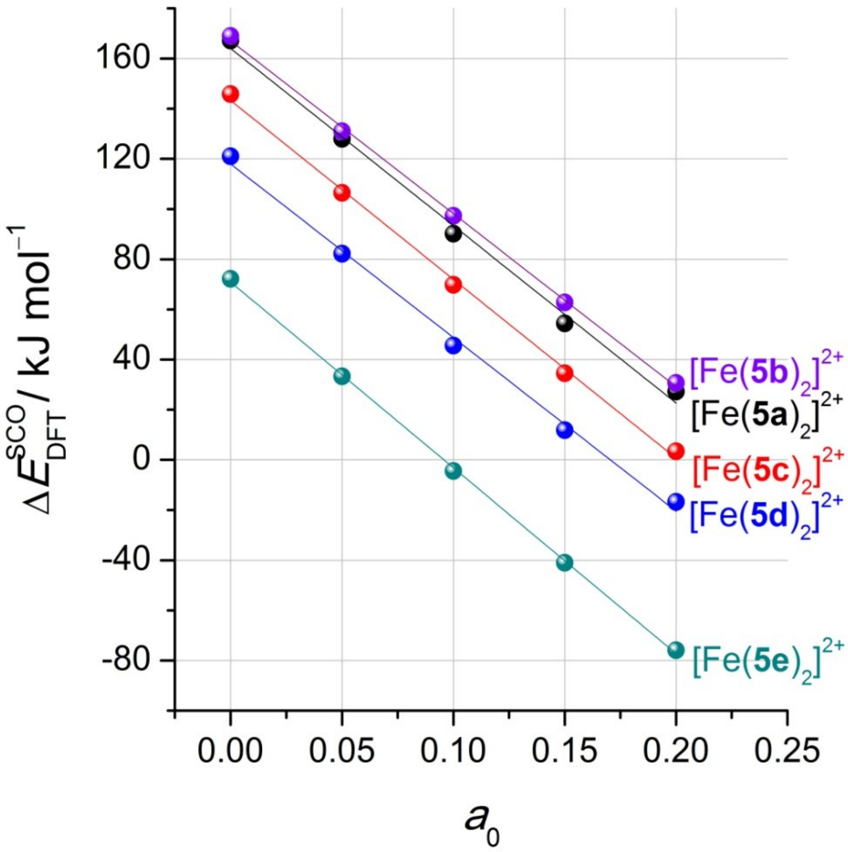

Figure 1-SI: DFT-derived (B3LYP-D/TZVPP) apparent SCO energies of complexes [Fe(**5**)$_2$]$^{2+}$ as a function of the amount of exact exchange a_0.

Table 1-SI: Fitting results of the linear regressions ($\Delta_{SCO}E = \Delta_{SCO}E^0 + (\delta_{SCO}E \times a_0)$) in Figure 1-SI.

[Fe(**5**)$_2$]$^{2+}$	$\Delta_{SCO}E^0$ (kJ mol^{-1})	$\delta_{SCO}E$ (kJ mol^{-1})	R^2
5a	164.1 ± 3.3	707 ± 27	0.9942
5b	167.1 ± 1.4	690 ± 11	0.9997
5c	143.3 ± 2.2	713 ± 18	0.9976
5d	118.0 ± 2.8	692 ± 23	0.9956
5e	70.9 ± 1.1	741 ± 9	0.9994

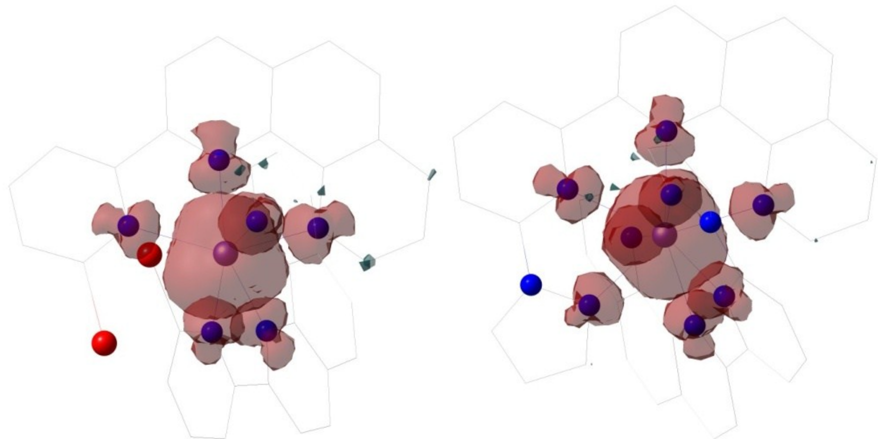

Figure 2-SI: DFT-computed spin-density distributions of the HS forms of $[Fe(\mathbf{5d})_2]^{2+}$ (left)and $[Fe(\mathbf{5e})_2]^{2+}$ (right).

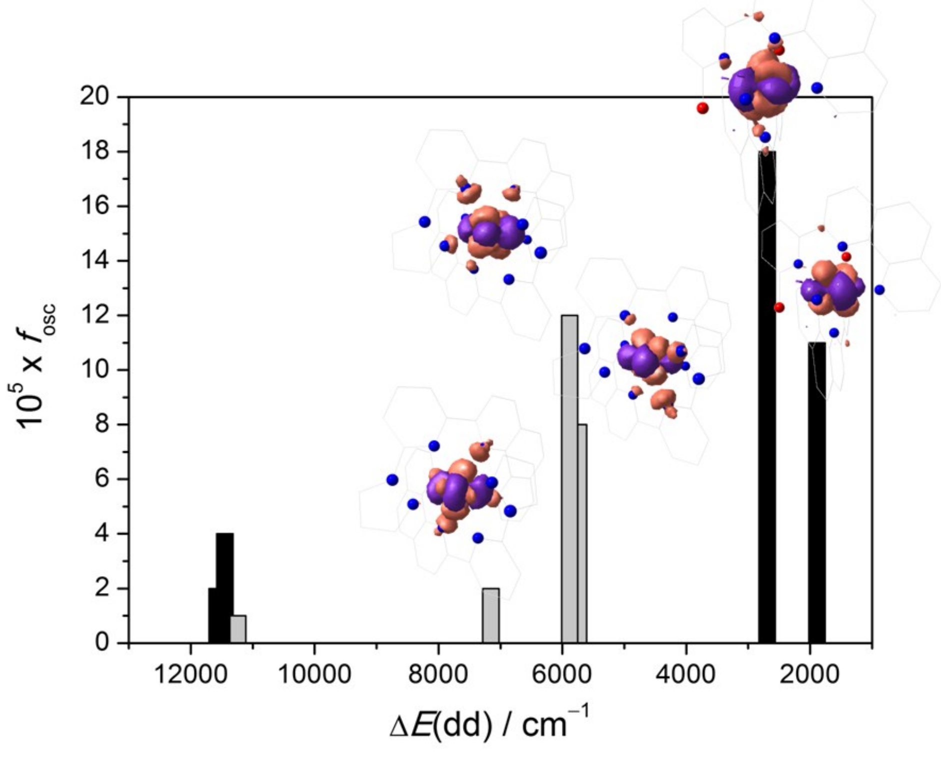

Figure 3-SI: TD-DFT-computed low-energy electronic transitions of dd character in $[Fe(\mathbf{5d})_2]^{2+}$ (black) and $[Fe(\mathbf{5e})_2]^{2+}$ (grey); orbital sketches denote the difference electron densities of the respective transition (blue: ground state; red: excited state).

1.3 SQUID measurements

Magnetic susceptibility data were collected by using a Quantum Design MPMS-XL SQUID magnetometer under an applied field of 0.5 T over the temperature range 5 to 400 K in the settle mode. The samples were placed in gelatine capsules held within a plastic straw. The data were corrected for the diamagnetic magnetisation of the ligands by using tabulated Pascal's constants and of the sample holder. The powder sample of $[Fe(\mathbf{5d})_2](BF_4)_2 \cdot n(CH_3CN)$ was stored for several days at ambient temperature in an open vessel what led to a partial loss of solvent. In general powders of $[Fe(\mathbf{5d})_2](BF_4)_2 \cdot n(CH_3CN)$ loose the solvent within few days at ambient temperature. This process can be monitored by the loss of the intensive violet colour that appears for freshly precipitated samples upon cooling in liquid nitrogen.

1.4 Mössbauer spectra

^{57}Fe Mössbauer spectra were recorded in transmission geometry with constant-accelaration using a conventional Mössbauer spectrometer with a 50 mCi ^{57}Co(Rh) source. The samples were sealed in the sample holder in an argon atmosphere. The spectra were fitted using Recoil 1.05 Mössbauer Analysis Software.[11] The isomer shift values are given with respect to a α-Fe reference at room temperature.

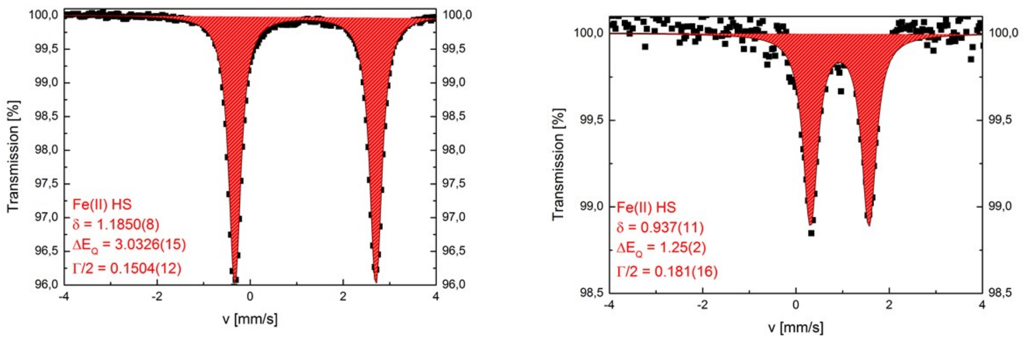

Figure 4-SI: Mössbauer spectrum of left) [Fe(**5e**)$_2$] (ClO_4)$_2$ and right) [Fe(**5d**)$_2$](ClO_4)$_2$ recorded at ambient temperature.

1.5 Cyclic voltammetry

Acetonitrile (analytical grade) was available from Acros Organics and stored over molecular sieve (4 Å). [N^{n}Bu$_4$][B(C_6F_5)$_4$] was prepared by metathesis of Li[B(C_6F_5)$_4$]·nEt$_2$O (Boulder Scientific) with [N^{n}Bu$_4$]Br according to a published procedure.[12] Its purification was enhanced by a filtration step of the crude product through a pad of silica using dichloromethane as a solvent.

For electrochemical measurements, a Voltalab 10 electrochemical laboratory from Radiometer Analytical was used. All experiments were carried out under an atmosphere of argon on acetonitrile solutions of the analyte (≈1 mM), containing 0.1 mol·L^{-1} of [N^{n}Bu$_4$][B(C_6F_5)$_4$] as supporting electrolyte.[13,14] For voltammetry, a three electrode cell with a platinum auxiliary electrode, a glassy carbon working electrode (3.0 mm in diameter) and a Ag/Ag$^+$ reference electrode were used. The working electrode was prepared by polishing with Buehler MicroFloc using Buehler diamond suspensions with decreasing sizes (1 to 0.25 µm). The Ag/Ag$^+$ reference electrode was constructed from a silver wire inserted into a Luggin capillary with a Vycor tip containing a solution of 0.01 mol·L^{-1} [$AgNO_3$] and 0.1 mol·L^{-1} of the supporting electrolyte in acetonitrile. This Luggin capillary was inserted into a second Luggin capillary with a Vycor tip filled with a 0.1 mol·L^{-1} supporting electrolyte solution in acetonitrile. Successive experiments under the same experimental conditions showed that all formal reduction and oxidation potentials were reproducible within ±5 mV. Experimental potentials were referenced against an Ag/Ag$^+$ reference electrode. Decamethylferrocene was used as an internal standard for potential adjustment and the experimentally measured potentials were converted into *E vs* FcH/FcH$^+$ as required by IUPAC[15] by addition of –0.51 V.[16,17] The cyclic voltammograms were taken typically after two scans and are considered to be steady state cyclic voltammograms, in which the signal pattern differs not from the initial sweep. Finally, the experimental data were processed on Microsoft Excel worksheets.

1.6 X-ray analysis

Suitable crystals of all investigated compounds were obtained by slow vapor diffusion of diethyl ether to a solution of the respective complex in acetonitrile.

1.6.1 Data recording and refinement

Diffraction data have been collected on an Oxford Gemini S diffractometer with graphite-monochromatized Mo Kα radiation (λ = 0.71073 Å). All structures were solved by direct methods and refined against $|F_o|^2$ with SHELXS-2013 and SHELXL-2013,[18] respectively (Table 2/Table 3). All non-hydrogen atoms were refined anisotropically. Hydrogen atoms were placed at calculated positions with a riding model.

In case of [Fe(**5a**)$_2$](BF$_4$)$_2$·2(CH$_3$CN), both BF$_4^-$ anions are disordered and have been refined to split occupancies of 0.59/0.41 (B1, F1-F4) and 0.65/0.35 (B2, F5-F8).

In case of [Fe(**5c**)](BF$_4$)$_2$ the command SQUEEZE has been used to generate a solvent-masked .hkl file. As indicated in the final .cif file packing solvent molecules occupy a solvent accessible volume of 1384 Å^3 in the unit cell with an accompanying electron count of 348. That corresponds well to the presence of 4 · diethyl ether and 8 · acetonitrile molecules as packing solvents with an expected electron count of 344, although all trials to refine these packing solvents reliable failed.

In order to record the HS state structure of [Fe(**5d**)$_2$](BF$_4$)$_2$·2(CH$_3$CN) (HS) the selected single crystal used for the measurement at 110 K was reused and crystal cooling was switched off. During this new measurement a slight decay of intensities was recognized, attributed to the loss of MeCN molecules as packing solvents. Eventually and suddenly close to the end of the data collection the crystal under measurement disintegrated completely. Identical observations were made when measuring other crystals of [Fe(**5d**)$_2$](BF$_4$)$_2$·2(CH$_3$CN) at room temperature. Due to this, data sets containing max. 95% data completeness were obtained. The given data refer to the first room temperature measurement of [Fe(**5d**)$_2$](BF$_4$)$_2$·2(CH$_3$CN), as this crystal represents the one of which the low-spin modification was determined before.

Table 2-SI: data for crystal structure refinement.

2	[Fe(**5a**)$_2$](BF$_4$)$_2$ ·2(CH$_3$CN)	[Fe(**5c**)$_2$](BF$_4$)$_2$	[Fe(**5d**)$_2$](BF$_4$)$_2$ ·2(CH$_3$CN) (LS)	[Fe(**5d**)$_2$](BF$_4$)$_2$ ·2(CH$_3$CN) (HS)	[Fe(**5e**)$_2$](BF$_4$)$_2$ ·3(CH$_3$CN)	[Zn(**5e**)$_2$](ClO$_4$)$_2$ ·3(CH$_3$CN)
CCDC-Nr.	1519515	1519516	1519517	1519518	1519519	1538100
empirical formula	$C_{34}H_{22}B_2F_8FeN_6$ ·2(CH$_3$CN)	$C_{36}H_{26}B_2F_8FeN_6O_2$	$C_{34}H_{20}B_2F_8FeN_6$ ·2(CH$_3$CN)	$C_{34}H_{20}B_2F_8FeN_6$ ·2(CH$_3$CN)	$C_{40}H_{26}B_2F_8FeN_{10}$ ·3(CH$_3$CN)	$C_{40}H_{26}Cl_2N_{10}O_8Zn$ ·3(CH$_3$CN)
formula weight (g/mol)	826.15	804.10	983.96	983.96	999.34	1034.14
T (K)	101(2)	110 K	110 K	298 K	110 K	110 K
Wavelength (Å)	0.71073	0.71073	0.71073	0.71073	0.71073	0.71073
cryst. sys. space group	triclinic *P-1*	monoclinic *P*2$_1$/c	triclinic *P-1*	triclinic *P-1*	triclinic *P-1*	monoclinic *P*2$_1$/n
unit cell dimensions						
a (Å)	11.5432(5)	15.7622(6)	11.8218(4)	12.0740(10)	12.5860(5)	14.7030(4)

b (Å)	11.9637(9)	12.2746(3)	11.8771(6)	12.2201(8)	12.6635(4)	14.7863(3)
c (Å)	14.2066(10)	24.0938(8)	14.6612(7)	14.8271(8)	14.9829(5)	21.1329(5)
α (°)	90.196(6)	90	92.953(4)	81.490(5)	96.447(3)	90
β (°)	95.816(5)	107.441(4)	97.763(3)	86.353(5)	100.639(3)	103.007(2)
γ (°)	113.065(6)	90	114.772(4)	113.602(7)	110.225(4)	90
volume	1793.8(2)	4447.2(3)	1838.58(15)	1964.3(3)	2161.73(14)	4476.48(19)
Z	2	4	2	2	2	4
absorption coefficient (cm^{-1})	0.505	0.407	2.668	2.497	0.437	0.740
F(000)	840	1632	976	976	1020	2120
Θ-range f. data coll. (°)	2.886 to 28.578	3.028 to 25.000	3.239 to 24.999	3.054 to 25	2.921 to 24.999	2.927 to 24.998
limiting indices	-14 ≤ h ≤ 14 -14 ≤ k ≤ 14 -18 ≤ l ≤ 18	-18 ≤ h ≤ 18 -14 ≤ k ≤ 14 -28 ≤ l ≤ 28	-14 ≤ h ≤ 14 -12 ≤ k ≤ 14 -16 ≤ l ≤ 17	-14 ≤ h ≤ 8 -14 ≤ k ≤ 14 -17 ≤ l ≤ 17	-14 ≤ h ≤ 14 -12 ≤ k ≤ 15 -17 ≤ l ≤ 17	-17 ≤ h ≤15 -17 ≤ k ≤ 17 -25 ≤ l ≤ 25
reflections coll. / unique	14154 / 7643 [R_{int} = 0.0340]	36979 / 7815 [R_{int} = 0.0425]	12559 / 6431 [R_{int} = 0.0281]	11687 / 6525 [R_{int} = 0.0459]	15107 / 7558 [R_{int} = 0.0354]	24690 / 7873[R_{int} = 0.0338]
data / restraints / parameters	7643/493/606	7815/569/543	6431/64/545	6525/91/580	15107/148/632	7873 / 0 / 634
GooF on F^2	1.063	1.054	1.031	0.968	1.073	1.037
final R indices ($I > 2\sigma(I)$)	$R1$ = 0.0694 w$R2$ = 0.1780	$R1$ = 0.0495 w$R2$ = 0.1206	$R1$ = 0.0330 w$R2$ = 0.0792	$R1$ = 0.0653 w$R2$ = 0.1866	$R1$ = 0.0829 w$R2$ = 0.1877	$R1$ = 0.0358 w$R2$ = 0.0795
(all data)	$R1$ = 0.0837 w$R2$ = 0.1883	$R1$ = 0.0641 w$R2$ = 0.1257	$R1$ = 0.0408 w$R2$ = 0.0826	$R1$ = 0.1120 w$R2$ = 0.2636	$R1$ = 0.1026 w$R2$ = 0.1979	$R1$ = 0.0494 w$R2$ = 0.0837
larg. diff. peak and hole ($e^-/Å^3$)	1.170 and -0.666	0.780 and -0.382	0.838 and -0.411	0.665 and -0.634	1.735 and - 1.025	0.329 and -0.318

2.1.1 Selected bond lengths and angles

Table 3-SI: Selected bond lengths (Å) and angles (°) in the solid state structures of $[Fe(\mathbf{5})_2](BF_4)_2$

	$[Fe(\mathbf{5a})_2](BF_4)_2 \cdot 2(CH_3CN)$	$[Fe(\mathbf{5c})_2](BF_4)_2$	$[Fe(\mathbf{5d})_2](BF_4)_2 \cdot 2(CH_3CN)$ (LS)	$[Fe(\mathbf{5d})_2](BF_4)_2 \cdot 2(CH_3CN)$ (HS)	$[Fe(\mathbf{5e})_2](BF_4)_2 \cdot 3(CH_3CN)$	$[Zn(\mathbf{5e})_2](ClO_4)_2 \cdot 3(CH_3CN)$
bond lengths (Å)						
Fe-N1	2.004(3)	1.993(2)	2.001(2)	2.211(6)	2.279(4)	2.1608(17)
Fe-N2	1.875(3)	1.879(2)	1.886(2)	2.091(5)	2.297(4)	2.0387(18)
Fe-N3	1.980(3)	2.028(2)	2.047(2)	2.219(6)	2.424(4)	2.4806(17)
Fe-N5					2.411(4)	4.65
Fe-N4/6*	1.998(3)	1.994(2)	2.009(2)	2.211(5)	2.348(4)	2.1534(18)
Fe-N5/7*	1.882(3)	1.884(2)	1.885(2)	2.094(5)	2.314(4)	2.0413(18)
Fe-N6/8*	1.993(3)	2.026(2)	2.077(2)	2.251(5)	2.367(4)	2.4489(17)
Fe-N10					2.355(4)	4.60
angles (°)						
N1-Fe-N4/6*	91.11(11)	91.91(9)	92.59(9)	93.6(2)	90.89(14)	118.16(6)
N2-Fe-N5/7*	179.07(12)	174.50(10)	169.61(10)	162.0(2)	141.26(14)	175.30(7)
N3-Fe-N6/8*	91.47(12)	93.83(9)	92.71(9)	98.6(2)	83.11(13)	77.30(6)
N1-Fe-N3	161.22(12)	160.79(8)	160.41(9)	148.2(2)	138.28(14)	149.24(6)
N4/6*-Fe-N6/8*	160.61(13)	160.86(9)	160.10(9)	148.1(2)	138.05(13)	148.81(6)

* due to different number of nitrogen atoms in the ligands **5a,c,d**/**5e** different numbering arise for equivalent N in $[Fe(\mathbf{5a,c,d})_2]^{2+}$/$[Fe/Zn(\mathbf{5e})_2]^{2+}$.

Table 4-SI: Selected bond lengths (Å) and angles (°) (**LS** / HS) in the DFT-optimized[a] structures of $[Fe(\mathbf{5})_2]^{2+}$.

	$[Fe(\mathbf{5a})_2]^{2+}$	$[Fe(\mathbf{5b})_2^{2+}$	$[Fe(\mathbf{5c})_2]^{2+}$	$[Fe(\mathbf{5d})_2]^{2+}$	$[Fe(\mathbf{5e})_2]^{2+}$
	LS / HS	**LS** / HS	**LS** / HS	**LS** / HS	LS / **HS**
bond lengths (Å)					
$Fe-N_{term}$	**2.036** / 2.271	**2.032** / 2.265	**2.021** / 2.269	**2.039** / 2.274	1.995 / **2.375**
$Fe-N_{cent}$	**1.898** / 2.137	**1.899** / 2.133	**1.902** / 2.136	**1.913** / 2.137	1.888 / **2.320**
$Fe-N_{pyr}$	**2.008** / 2.216	**2.002** / 2.223	**2.053** / 2.201	**2.107** / 2.251	2.035 / **2.376**
$Fe-N_{pyrazol}$					3.560 / **2.348**
$Fe-N_{term'}$	**2.032** / 2.273	**2.029** / 2.232	**2.029** / 2.286	**2.034** / 2.265	1.997 / **2.343**
$Fe-N_{cent'}$	**1.897** / 2.137	**1.899** / 2.134	**1.903** / 2.133	**1.914** / 2.137	1.888 / **2.318**
$Fe-N_{pyr'}$	**2.010** / 2.222	**2.007** / 2.209	**2.061** / 2.207	**2.113** / 2.252	2.033 / **2.378**
$Fe-N_{pyrazol}$					3.564 / **2.350**
angles (°)					
$N_{pyr}-Fe-N_{pyr'}$	**91.5** / 94.5	**91.4** / 91.6	**89.4** / 94.9	**91.5** / 99.5	88.6 / **132.1**
$N_{cent}-Fe-N_{cent'}$	**178.5** / 176.4	**179.2** / 161.1	**172.7** / 157.0	**168.3** / 155.2	170.3 / **140.9**

N_{term}-Fe-N_{term}	**91.5** / 87.3	**90.4** / 87.4	**90.8** / 85.5	**91.3** / 88.2	89.88 / **91.1**
N_{pyr}-Fe-N_{term}	**160.7** / 146.9	**161.1** / 146.4	**159.8** / 147.3	**159.2** / 147.2	160.1 / **137.7**
$N_{pyr'}$-Fe-$N_{term'}$	**160.7** / 146.9	**161.0** / 147.5	**159.8** / 147.2	**159.2** / 147.3	160.0 / **137.5**

[a] Optimization on the B3LYP*-D/TZVP level of theory; bold numbers are given for the experimentally observable species; the indices *term*, *cent* and *pyr* denote the donor atom locations in the terminal and central rings of the phenanthroline and in the pyridine ring, respectively.

2.1.2 Quantification of the distortion - Continuous Shape Measure (CShM)[19,20]

The SHAPE module on the respective webpage was used to quantify the shape and symmetry of the polyhedra.[19,21] „The shape measure evaluates the degree of polyhedricity in distorted polyhedra. Perfect polyhedra are highly symmetric, and therefore in its application here, shape is also a symmetry measure.“ „The value of this measure ranges from zero - the molecule has the investigated polyhedral shape - to higher values (the upper limit is 100); the higher the shape-measure value, the farther is the structure from the reference shape.“ [19,21] To calculate the measure for octahedral and trigonal prismatic reference polyhedra from Professor Avnir’s web page at the University of Jerusalem were used. Reference polyhedra for the trigonal dodecahedron (DD) and square antiprism (SAPR) have been calculated, the positions are given in the Table 5-SI.

The elucidation of the reference polyhedron for [Fe(**5e**)$_2$]$^{2+}$ deserves special attention. The two most common polyhedra for eight coordinated complexes are the square-antiprism[22] and the trigonal dodecahedron.[23] In terms of Coulomb repulsion, the square-antiprism minimizes ligand-ligand interaction. However, the *N*-donors in [Fe(**5e**)$_2$]$^{2+}$ are bonded to a rigid ligand backbone that prefers a planar structure to maximize resonance effects in the aromatic system. This causes considerable deviations from an ideal square antiprism (S_{SAPR} = 3.89). A better reference polyhedron is the trigonal dodecahedron with D_{2d} symmetry. This polyhedron is constructed by locating each of the four donors of one ligand (N1,N2,N3,N5 and N6,N7,N8,N10) on one of two perpendicular meridians around the metal ion. The positions of the donors on the meridian are chosen to give identical distances between the donors on the meridian and between the inner and terminal donors close to the intersection of the two meridians. For an ideal trigonal dodecahedron the ratio between the Fe-N bond lengths and distance between adjacent N-donors is 1.19. The N-Fe-N angle between adjacent N-donors is 73.7°.[24] This polyhedron is in good accordance with the structure of [Fe(**5e**)$_2$]$^{2+}$ (S_{DD} = 1.36).

Table 5-SI: Coordinates for reference polyhedra used in the CShM calculations.

polyhedron	square antiprism (SAPR) (M-D = 0.824 and adjacent D-D = 1)			trigonal dodecahedron (DD) (M-D = 1 and adjacent D-D on same meridian = 1.199)		
	x	y	z	x	y	z
D1	0.7071	0	-0.423	-0.9364	0	0.3509
D2	0	0.7071	-0.423	-0.5997	0	-0.8002
D3	-0.7071	0	-0.423	0.5997	0	-0.8002
D4[a)]	0	-0.7071	-0.423	0.9364	0	0.3509
D5	0.5	0.5	0.423	0	0.9364	-0.3509
D6	-0.5	0.5	0.423	0	0.5997	0.8002
D7	-0.5	-0.5	0.423	0	-0.5997	0.8002
D8[a)]	0.5	-0.5	0.423	0	-0.9364	-0.3509
M	0	0	0	0	0	0

a) omitted for calculation on dodecahedral symmetry on distorted octahedral complexes [Fe(**5a,c,d**)$_2$]$^{2+}$

Table 6-SI: Calculated CSM of the complexes [Fe(**5a,c-e**)$_2$]$^{2+}$ in solid state.

	Fe-N largest and shortest (Å)	CShM $S_{OC\text{-}6}$ octahedron (O_h)	CShM $S_{TP\text{-}6}$ trigonal prism w. cent. atom (D_{3h})	CShM S_{SAPR} square antiprism w. centr. Atom (D_{4d})	CShM S_{DD} trigon. dodecaeder centr. atom [b)] (D_{2d})
[Fe(**5a**)$_2$](BF_4)$_2$ (LS)	1.87-2.00	1.96	12.13		7.18
[Fe(**5c**)$_2$](BF_4)$_2$ (LS)	1.88-2.03	2.20	11.31		5.69
[Fe(**5d**)$_2$](BF_4)$_2$ (LS)	1.88-2.08	2.64	9.98		4.88
[Fe(**5d**)$_2$](BF_4)$_2$ (HS/RT)	2.09-2.25	6.22	7.86		3.43
[Fe(**5e**)$_2$](BF_4)$_2$ (HS)	2.28-2.42	12.21[a)]	9.46	3.89	1.37
[Zn(**5e**)$_2$](ClO_4)$_2$	2.04-2.48	6.60	10.50		

a) the two pyrazol donor nitrogen atoms have been omitted

b) for all complexes, except [Fe(**5e**)$_2$](BF_4)$_2$, two donors have been omitted in the reference polyhedron

2.2 Laser flash photolysis (LFP)

Nanosecond LFP experiments were performed with the laser wavelength 532 nm of a Nd:YAG laser system, as described in detail elsewhere.[25] Decay profiles of transient absorption of [Fe(**5c**)$_2$]$^{2+}$ were recorded in acetonitrile at λ_{obs} = 570 nm, corresponding to the maximum of the ground-state MLCT absorption of the complex ions. The pulse duration of 10 ns with energy of *ca.* 2-3 mJ per pulse was much shorter than the decay lifetimes of the transient signals, so that deconvolution was not required for kinetic analysis. Before the measurement, the solution in high-purity acetonitrile (OD_{532} ≈ 0.5; concentrations in the range 1×10^{-4} M) were rigorously deoxygenated by flushing with analytical grade argon for 20 minutes prior to measurement, under argon, in sealed quartz cuvettes. The observed relaxation rates k_{ex} were split into the $k_{HS\rightarrow LS}$ and $k_{LS\rightarrow HS}$ with thermodynamic parameters obtained by interpretation of the chemical shifts of the ^1H NMR spectra in acetone solution ($T_{½}$ = 345 K and $\Delta_{SCO}S$ = 81.5 J/mol·K).

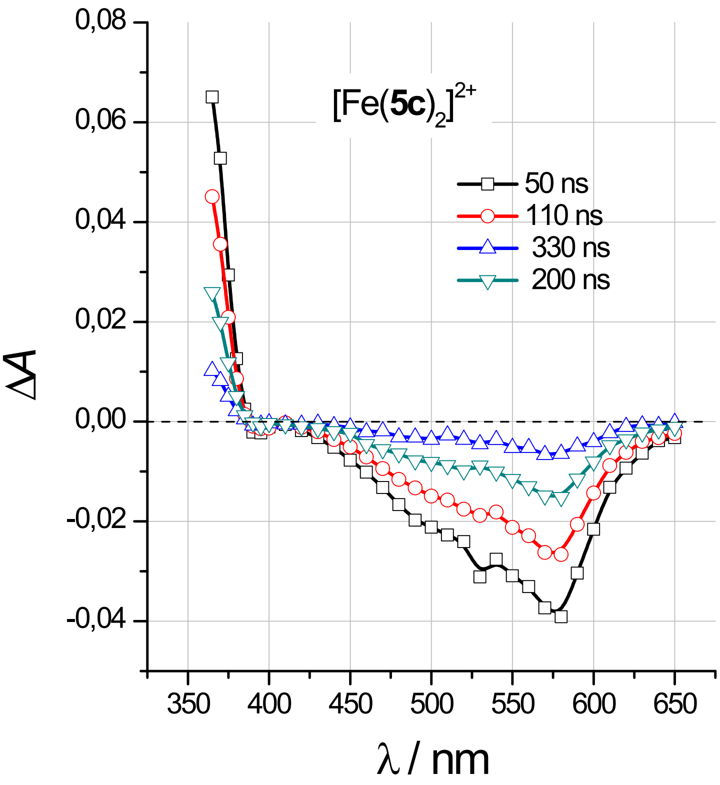

Figure 5-SI: Transient absorption spectra recorded at time delays of 50-200 ns after the laser flash (λ_{exc} = 532 nm; 9 ns; 2-3 mJ) c = 10^{-4} M (acetonitrile at 298 K).

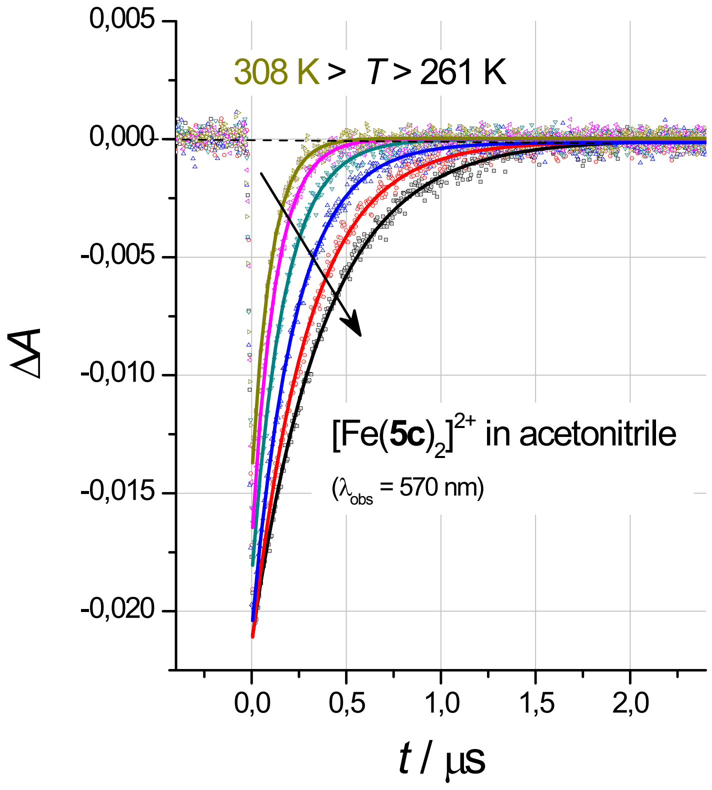

Figure 6-SI: Temperature dependence of the relaxation dynamic; λ_{obs} = 580 nm. The lines represent the best fit to a mono exponential decay.

Table 7-SI: Recorded SCO exchange rate constants k_{ex} from the FLP-experiments on $[Fe(\mathbf{5c})_2]^{2+}$ in acetonitrile solution. With the assumption of $T_{½}$ = 345 K and $\Delta_{SCO}S$ = 81.5 J/mol·K, forward and backward processes were isolated. Arrhenius fitting: $E_{a(LS\rightarrow HS)}$ = 43 kJ/mol; $A_{LS\rightarrow HS} = 4.8\cdot10^{13}$ s^{-1}; $E_{a(HS\rightarrow LS)}$ = 15 kJ/mol; $A_{HS\rightarrow LS} = 2.66\cdot10^{10}$ s^{-1}.

***T* (K)**	**k_{ex} (10^6 s^{-1})**	**γ_{HS}**	**$k_{LS\rightarrow HS}$ (10^6 s^{-1})**	**$k_{HS\rightarrow LS}$ (10^6 s^{-1})**
258	2.63	0.0349	0.09	2.53
268	3.22	0.0557	0.179	3.04
278	4.17	0.0850	0.355	3.82
288	5.56	0.124	0.690	4.87
298	7.69 (7.94*)	0.174	1.34	6.35
308	10.0	0.233	2.33	7.67

* in acetone solution

2.3 VT-^{1}H NMR spectroscopy

2.3.1 General remarks on ^{1}H NMR spectroscopic methods

NMR spectra were recorded on a 500 MHz Bruker Avance III spectrometer. If not otherwise noted, temperatures were corrected by calibration with external anhydrous methanol or anhydrous ethylene glycol samples using calibration functions from the literature.[26]

A full signal assignment of the complexes in their paramagnetic HS state especially $[Fe(\mathbf{5e})_2]^{2+}$ is not possible. Nevertheless, the number of found proton resonances and the integrated intensities are in excellent agreement with the implications of C_2 symmetry in solution. For all calculation we expected Curie-like behavior of pure HS-complexes. The temperature dependence of the Curie constant $C(T)$ is accounted by the first order correction using C^1 ($C(T) = C^0+C^1\cdot T$). Hence the temperature dependence of chemical shift of the proton resonances can be expressed by the equation (1). A detailed justification for this approach is found the literature.[27]

$$\delta_{obs}(T) = C^0\frac{1}{T} + C^1 + \delta_{dia} \tag{1}$$

In this relation C^0 represents the Curie constant and C^1 represents the first-order correction term for the temperature dependence of the Curie constant and δ_{dia} represents the diamagnetic contribution. From the actual measurement, only the sum of C^1 and δ_{dia} can be obtained. Clearly, however, the intercept of the Curie plots at $1/T$ = 0 K^{-1} does not solely represent δ_{dia}. To account for the difference to reasonable values C^1 is needed. With this approach, excellent agreement of calculated and observed shifts is obtained with deviations smaller than 0.2 ppm (*vide infra*). For calculations of relaxivities, asymmetric two side exchange and fitting of the chemical shifts a Excel-scripts from the NMR$_2$SCO package, available from the author's homepage,[28] were used.

2.3.2 ^{1}H NMR spectra of $[Fe(5d)_2]^{2+}$ in d_5-nitrobenzene (internal temperature reference)

In order to validate the C^1-correction model (1) for the HS-Fe^{2+} complex $[Fe(\mathbf{5d})_2]^{2+}$, NMR experiments were conducted in d_5-nitrobenzene solution with an internal temperature reference. The temperature reference was a coaxial inset tube filled with anhydrous ethylene glycol. The difference in the chemical shift between the OH- and CH_2-signal serves as temperature reference. Calibration functions to convert the chemical shift difference (Δ $(\delta_{OH}$-$\delta_{CH2})$ into temperatures are available in the literature.[26,29] In order to improve the baseline stability, spectra were only recorded with limited sweep width; as a consequence, the protons *H*1 and *H*7 are excluded from this survey. Resonances were assigned by $^1H,^1H$-COSY spectra and the T_1 times. Raw data are listed in Table 8. It should be pointed out that the residuals are indeed very small ($\Delta\delta < 0.15$ ppm) and the curves are slightly bent. The latter feature points to a minor systematic deviation from the C^1-approximation (1). Several reasons might be given, for instance incorrect temperature referencing or a possible SCO. However, the deviations are so small that they do not hold any useful information.

Table 8-SI: Source ^{1}H-NMR data for [(Fe(**5d**)$_2$]$^{2+}$] in d_5-nitrobenzene solution.

T_{corr} (°C)	T_{set} (°C)	δ_{OH} (ppm)	δ_{CH2} (ppm)	Δ (δ_{OH}-δ_{CH2}	T_{corr} (K)	1/T_{corr} (1/K)	*H*6 (ppm)	*H*9 (ppm)	*H*4/5 (ppm)	*H*3 (ppm)	*H*4/5 (ppm)	*H*2 (ppm)	*H*10/8 (ppm)	*H*10/8 (ppm)
22.47	20	6.3439	3.3881	0.3958	295.62	0.003382	-21.193	15.889	16.405	22.150	26.131	58.776	63.202	64.941
27.71	25	6.2986	3.3941	0.3445	300.86	0.003323	-20.502	15.604	16.364	21.709	25.828	57.853	62.156	63.811
32.58	30	6.2563	3.3994	0.2969	305.73	0.003270	-19.884	15.352	16.327	21.315	25.555	57.022	61.212	62.801
37.67	35	6.2101	3.4029	0.2472	310.82	0.003217	-19.257	15.099	16.289	20.921	25.281	56.186	60.265	61.786
42.96	40	6.1645	3.409	0.1955	316.11	0.003163	-18.627	14.845	16.249	20.524	25.003	55.339	59.312	60.769
48.05	45	6.1207	3.415	0.1457	321.20	0.003113	-18.039	14.614	16.214	20.161	24.745	54.559	58.424	59.832
52.86	50	6.0778	3.4191	0.0987	326.01	0.00306	-17.507	14.403	16.178	19.829	24.509	53.843	57.615	58.975
58.36	55	6.0293	3.4243	0.045	331.51	0.003016	-16.915	14.172	16.139	19.463	24.247	53.051	56.719	58.033
63.36	60	5.984	3.428	-0.004	336.52	0.002971	-16.399	13.968	16.102	19.143	24.017	52.355	55.935	57.213
73.35	70	5.8954	3.437	-0.1017	346.50	0.002885	-15.411	13.587	16.033	18.541	23.576	51.026	54.436	55.643
83.95	80	5.8001	3.4453	-0.2052	357.10	0.002800	-14.432	13.213	15.960	17.947	23.137	49.701	52.944	54.090
94.64	90	5.7042	3.4538	-0.3097	367.79	0.002718	-13.520	12.868	15.888	17.398	22.725	48.461	51.552	52.648
105.34	100	5.6073	3.4616	-0.4143	378.49	0.002642	-12.657	12.546	15.816	16.884	22.332	47.279	50.224	51.280
126.37	120	5.4158	3.4757	-0.6199	399.52	0.002502	-11.070	11.960	15.672	15.946	21.601	45.087	47.768	48.764

$$\delta_{obs}(x) = C^0 x + C^1 + \delta_{dia} \qquad \text{with } X = 1/T \qquad (2)$$

Table 9-SI: Results of linear fits of the ^1H chemical shift to *T* according to fit function (2) ([$[(Fe(\mathbf{5d})_2]^{2+}$] in d_5-nitrobenzene).

$[(Fe(\mathbf{5d})_2]^{2+}]$ in d_5-nitrobenzene	Intercept $C^1+\delta_{dia}$ Value (ppm)	Intercept $C^1+\delta_{dia}$ Standard Error (ppm)	Slope C^0 Value (ppm K)	Slope C^0 Standard Error (ppm K)	Statistics Adj. R-Square
H6	17.780	0.0792	-11510.5	26.26	0.99993
H9	0.710	0.0971	4472.3	32.18	0.99933
H4/5	13.657	0.0470	818.5	15.58	0.99531
H3	-1.801	0.1237	7061.7	41.01	0.99956
H4/5	8.746	0.0124	5139.2	4.09	0.99999
H2	6.212	0.0484	15532.6	16.05	0.99999
H10/8	3.900	0.0786	17519.1	26.04	0.99997
H10/8	2.689	0.2053	18369.4	68.07	0.99982

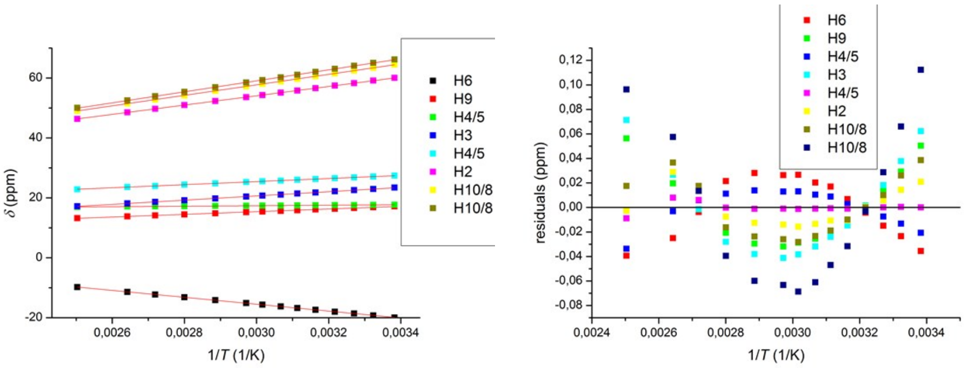

Figure 7-SI: Graphical representation of fit of ^1H-NMR data to 1/*T* according to to eq. (2); (left) fit; (right) residuals (both for $[Fe(\mathbf{5d})_2]^{2+}$ recorded in d_5-nitrobenzene).

$$\delta_{obs}(T)\, T = C^0 + (C^1 + \delta_{dia})\, T \qquad (3)$$

Table 10-SI: Results of the refinement of ^1H chemical shifts of $[Fe(\mathbf{5d})_2]^{2+}$ in d_5-nitrobenzene solution according to fit function (3).

$[(Fe(\mathbf{5d})_2]^{2+}]$ in d_5-nitrobenzene	Intercept C^0 Value	Intercept C^0 Standard Error	Slope $C^1+\delta_{dia}$ Value	Slope $C^1+\delta_{dia}$ Standard Error	Statistics Adj. R-Square
H6	-11495.51	25.80	17.74	0.08	0.99979
H9	4453.32	31.60	0.77	0.09	0.97332
H4/5	827.86	15.84	13.63	0.05	0.99987

H3	7037.58	40.35	-1.73	0.12	0.5
H4/5	5139.90	4.53	8.74	0.013	0.99998
H2	15527.09	15.81	6.23	0.047	0.99949
H10/8	17506.64	25.07	3.94	0.075	0.99736
H10/8	18331.05	65.55	2.80	0.195	0.97123

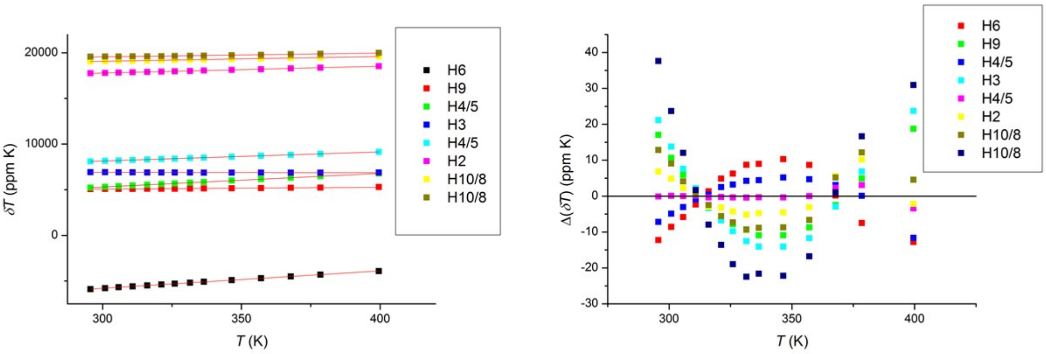

Figure 8-SI: Graphical representation of the fit of ^{1}H NMR data to T (d_5-nitrobenzene) according to eq. (3) for $[Fe(\mathbf{5d})_2]^{2+}$; (left) fit; (right) residuals

Table 11-SI: Results of the refinement of chemical shifts of $[Fe(\mathbf{5d})_2]^{2+}$ in d_6-acetone solution according to fit function (2).

$[(Fe(\mathbf{5d})_2]^{2+}]$ in d_6-acetone	Intercept $C^1 + \delta_{dia}$ Value	Intercept Standard Error	Slope C^0 Value	Slope Standard Error	Statistics Adj. R-Square
H6	16.45	0.92	-11171.14	213.10	0.99746
H9	13.45	0.48	797.84	110.86	0.87888
H4/5	-0.71	0.73	4934.38	168.47	0.9919
H3	-0.45	0.46	6871.91	106.37	0.99833
H4/5	7.54	1.06	5517.13	246.25	0.98622
H2	4.10	1.54	15980.44	357.01	0.99652
H10/8	3.00	1.47	17713.86	340.04	0.99743
H10/8	-6.56	2.35	20942.47	544.04	0.9953
H7	-9.16	2.63	30180.31	607.70	0.99717
H1	-63.86	7.26	78289.26	1678.80	0.99679

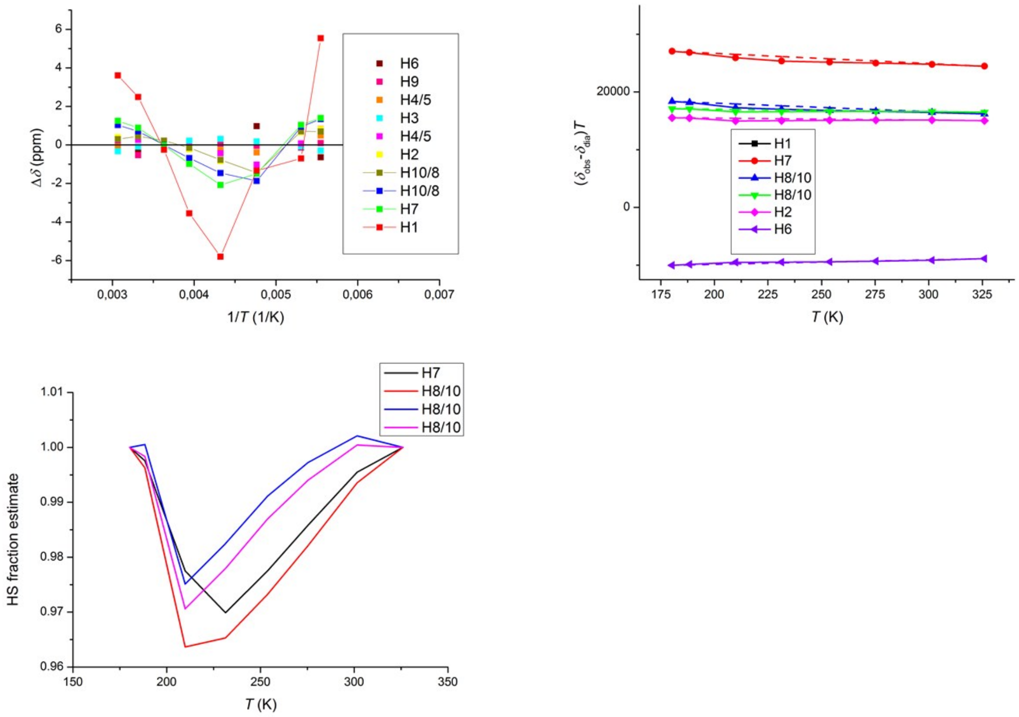

Figure 9-SI: top left) residuals of the fit to ^{1}H chemical shifts on $1/T$ for [Fe(**5d**)$_2$]$^{2+}$ in d_6-acetone solution; top right) dashed line represents the chemical shift of the pure HS state used for calculations and the solid line connects the experimental points. The difference is the result of SCO; bottom left) HS fraction calculated from the difference between pure HS state chemical shift and the observed shift; Please note that the coalescence occurs around 230 K. At this point, the signal set splits into HS and LS components that do not exchange on the NMR timescale: That is, the chemical shift of the HS component is then independent of the equilibrium (*apparent* return to γ_{HS} = 1.0) . The second set of resonances for the pure LS state is too weak in intensity (<10% of HS resonance) and too broad (>10 times broader than the HS resonance) to be observable.

2.3.3 Proton spin relaxation time (R_1) measurements and solution model for relaxivities (R_1/R_2) in [Fe(5d)$_2$]$^{2+}$

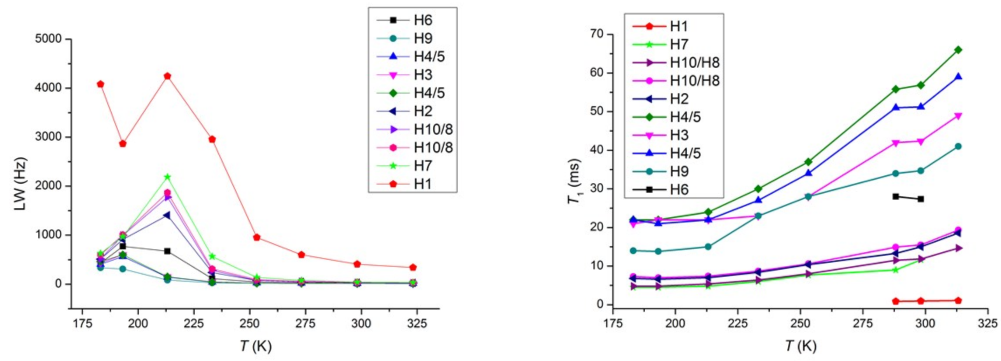

Figure 10-SI: left) Linewidths of resonances of [Fe(**5d**)$_2$]$^{2+}$; right) longitudinal relaxation times (T_1) for [Fe(**5d**)$_2$]$^{2+}$.

In order to obtain a consistent picture of the ^{1}H spectroscopic properties of the Fe^{2+} complexes, T_1 times (Figure 10-SI) were measured by the usual inversion recovery experiment. The T_1 times of complex [Fe(**5d**)$_2$]$^{2+}$ are in good accordance with a mainly dipolar relaxation mechanism and hence follow the T_1 ~ r^6 rule (r denotes the non-bonded distance of proton and iron centre; Figure 11-SI left). The proportions R_1/r^{-6} between relaxivity $1/T_1 = R_1$ and the distance r were calculated by plotting R_1 over r^{-6} and subsequent linear regression with the intercept fixed at (0,0). This proportion depends on the time constant of the electron relaxation τ_s. Hence, the time constant of the electron relaxation τ_s can be calculated from this proportion using Solomon-Bloembergen equation,[30] with the usual approximations for Fe^{2+} SCO complexes.[27] The Curie relaxation was also calculated by using tabulated viscosities for acetone and the assumption of a radius of 8 Å for [Fe(**5d**)$_2$]$^{2+}$. In general the Curie contribution to T_1 is less than 10 %. Results for R_1/r^{-6} and τ_s are presented in Figure 11-SI.

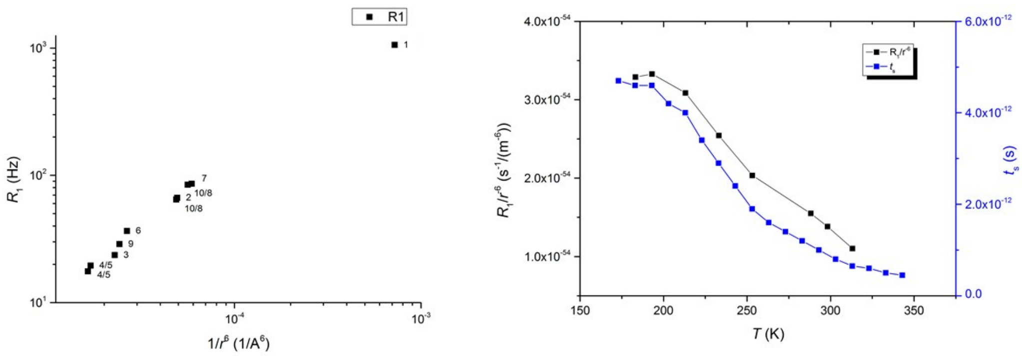

Figure 11-SI: left) Plot of the longitudinal relaxivity R_1 over 1/r^6 of complex [Fe(**5d**)$_2$]$^{2+}$(logarithmic scale was used for visual clarity); right) temperature dependence of R_1/r^{-6} and τ_s for complex [Fe(**5d**)$_2$]$^{2+}$.

The transversal relaxations R_2 were calculated by Solomon-Bloembergen equations[27,30]. For R_2 the Curie contribution becomes dominant at low temperatures. This is best seen for H1. H1 is the only proton where, at the lowest temperature, the calculated and experimental R_2 times agree within the model (Figure 12-SI). For proton *H*1 the Curie contribution is much larger than the exchange broadening due to the close vicinity of *H*1 to the HS Fe^{2+} ion (1/r^6 dependence). Otherwise, below 260 K, the R_2 values are significantly larger than expected from the model. The drop in the linewidths at T < 260 K is not consistent with the model for proton relaxation for pure HS Fe^{2+} complexes.[30] Moreover this discontinue is not reflected in the longitudinal relaxation $R_1 = 1/T_1$. The longitudinal relaxation R_1 increases continually with decreasing temperature (Figure 11). For many other reasons it is very unreasonable that the increased R_2 times are the result of a paramagnetic contribution. With realistic assumptions R_2 must continuously increase with decreasing temperature until either the rotational correlation time or the time constant for the electron relaxation are longer than 1/π *LW* (< 1ms). This is extremely unlikely at 170 K. It will be shown below that these deviations are indeed caused by the SCO.

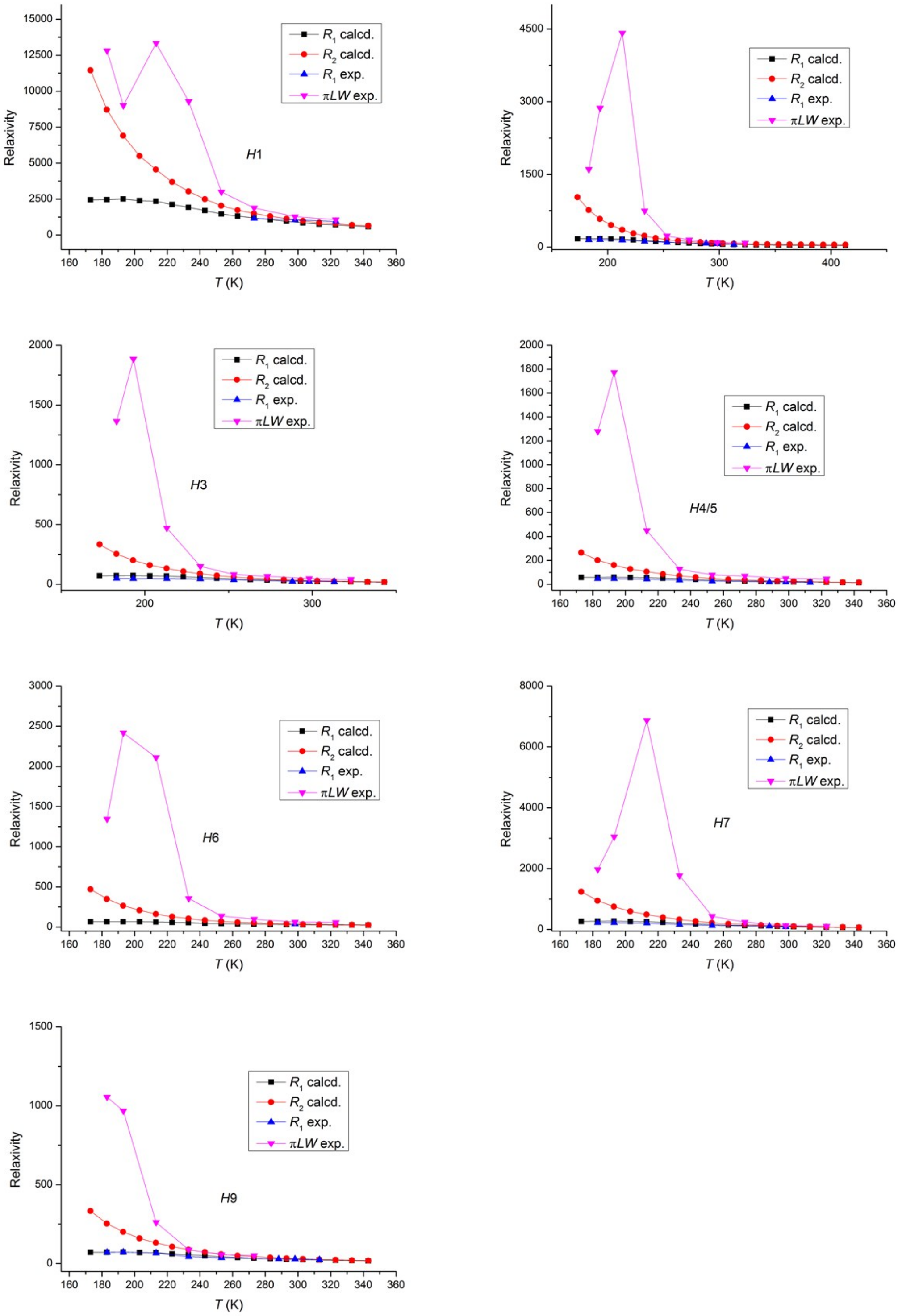

Figure 12-SI: Plots of temperature dependence of calculated and experimentally observed relaxivities R_1 and R_2 (in units of Hz) for protons of [Fe(**5d**)$_2$]$^{2+}$. The longitudinal relaxivities R_2 were calculated from LWs ($LW = R_2/\pi$).

Model calculations were performed to clarify the origin of the "SCO humps" in the temperature dependence of R_2 for [Fe(**5d**)$_2$]$^{2+}$. Relaxivities R_{2HS}, calculated for the pure HS state were used in the model calculations (*vide supra*). Transversal relaxivities R_{2LS} of the LS state were set to 0.1 Hz (T_{2LS} = 10s). The chemical shift differences between the LS and HS state, $\Delta\omega$, were calculated from fits on acetone solution samples (Table 11-SI). Chemical shifts of the proton resonances in [Fe(**5d**)$_2$]$^{2+}$ obtained for d_5-nitrobenzene solution were used to separate C^1 and δ_{dia}. The forward and backward rate constants of the SCO equilibrium $k_{HS\rightarrow LS}$ and $k_{LS\rightarrow HS}$ were calculated according to the Arrhenius model. In this model the frequency factor for the HS→LS reaction $A_{HS\rightarrow LS}$ was taken from kinetic data available from Laser Flash Photolysis studies on $[Fe(\mathbf{5c})_2]^{2+}$. Given the structural similarity of $[Fe(\mathbf{5c})_2]^{2+}$ and $[Fe(\mathbf{5d})_2]^{2+}$ and the structure-independence of Arrhenius frequency factors A in Fe^{2+} based SCO systems,[31,32] this data transfer appears justified. The frequency factor $A_{LS\rightarrow HS}$ for the reverse reaction was calculated by assuming an entropy difference of $\Delta_{SCO}S$ = 81.5 J/mol K as indicated from ^{1}H-NMR studies on $[Fe(\mathbf{5c})_2]^{2+}$:

$A_{LS\rightarrow HS} = A_{HS\rightarrow LS}\,(\Delta_{SCO}S/R)$. ($R$ = 8.314459 J/(mol K))

The activation barrier $E_{a(HS\rightarrow LS)}$ for the HS-LS reaction and $T_{1/2}$ were determined by testing. $E_{a(LS\rightarrow HS)}$ was calculated from $T_{1/2}$ and $E_{a(HS\rightarrow LS)}$:

$E_{a(LS\rightarrow HS)} = E_{a(HS\rightarrow LS)} + T_{1/2}\cdot\Delta_{SCO}S = E_{a(HS\rightarrow LS)} + \Delta_{SCO}H$.

This two site exchange was modeled using the Bloch-McConnell equations with no simplifications following previous work in this field.[28,33–35] Calculations were performed using the Visual Basic script **NMR$_2$SCO**[28] on Excel worksheets. The results obtained with settings of $T_{1/2}$ = 140 K and $E_{a(HS\rightarrow LS)}$ = 22.5 kJ/mol are in reasonable agreement with experimental results. In the light of the assumptions made these values should be regarded as preliminary estimates. Nevertheless, these results indeed show that this two-sites exchange satisfyingly mimics the "humps" and corroborates our assignment as a beginning SCO in $[Fe(\mathbf{5d})_2]^{2+}$.

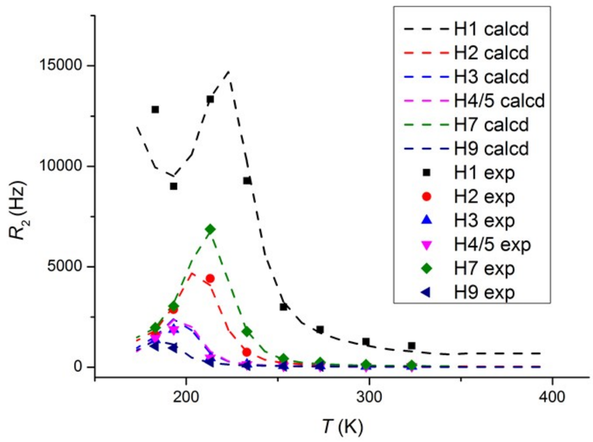

Figure 13-SI: Plot of the calculated transverse relaxivities R_2 (lines) and experimental data (symbols) for full treatment of two side exchange.

2.3.4 Chemical shifts and relaxivities of $[Fe(5e)_2]^{2+}$

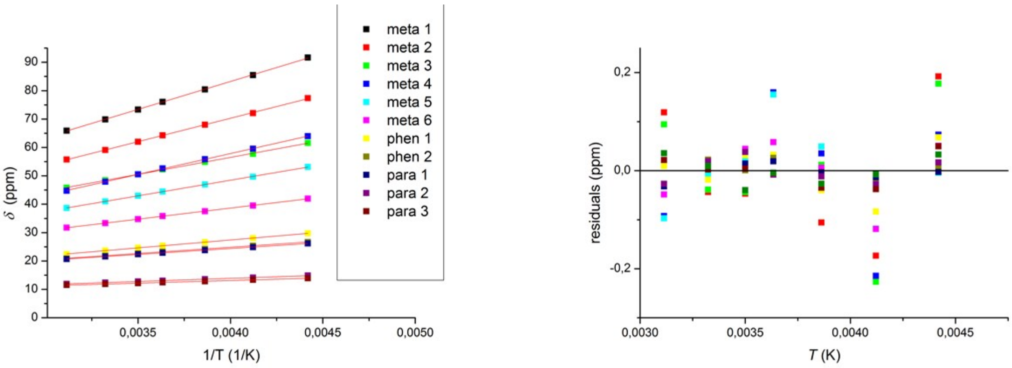

Figure 14-SI: Linear fits and residuals for chemical shifts of $[Fe(\mathbf{5e})_2]^{2+}$ with fit function (2).

Table 12-SI: Results of the refinement of chemical shifts of $[Fe(\mathbf{5e})_2]^{2+}$ in d_6-acetone solution according to fit function (2).

Proton	Intercept Value (ppm)	Intercept Standard Error (ppm)	Slope Value (ppm K)	Slope Standard Error (ppm K)	Statistics Adj. R-Square
meta 1	4.538	0.472	19673.95	126.35	0.99975
meta 2	4.323	0.463	16489.16	123.85	0.99966
meta 3	8.646	0.442	11961.60	118.26	0.99941
meta 4	-0.887	0.336	14682.90	89.97	0.99977
meta 5	4.373	0.234	11021.04	62.68	0.99981
meta 6	7.391	0.187	7811.99	50.05	0.99975
phen 1	5.193	0.076	5552.56	20.31	0.99992
phen 2	7.270	0.069	4394.00	18.48	0.99989
para 1	7.661	0.092	4184.54	24.65	0.99979
para 2	5.016	0.112	2220.50	29.96	0.99891
para 3	5.722	0.104	1849.18	27.71	0.99865

2.3.5 Thermodynamics from NMR - ^1H NMR data reduction for $[Fe(5c)_2]^{2+}$ *d_6-acetone solution*

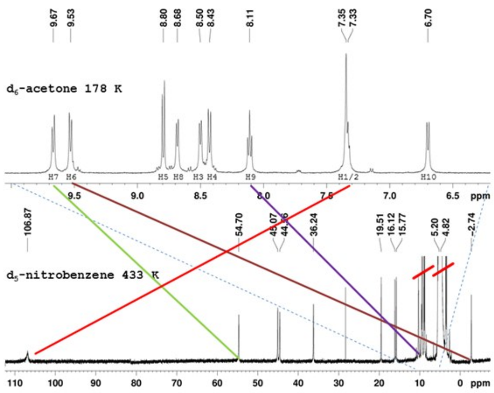

Figure 15-SI: ^1H NMR spectra of $[Fe(\mathbf{5c})_2]^{2+}$ at 173 K (top) and 433 K (bottom) in d_6 acetone demonstrate the transition from the LS to the HS state of the Fe^{2+} ion. The red bars mark the solvent residual protons and the external temperature reference (glycol). Lines are added as guide for the eye.

The thermodynamic data of SCO in [Fe(**5c**)$_2$]$^{2+}$ were calculated according to our recently published approach. C^1 parameters were fixed to values obtained from [Fe(**5d**)$_2$]$^{2+}$ by subtraction of δ_{dia}. The diamagnetic contributions δ_{dia} were fixed to the values of the parent diamagnetic complex [Fe(**5a**)$_2$]$^{2+}$ for the refinement in d_5-nitrobenzene and to the values found at 178 K for [Fe(**5c**)$_2$]$^{2+}$ in d_6-acetone solution. NMR parameters are given in Table 13-SI for d_6-acetone and Table 14-SI for d_5-nitrobenzene. Thermodynamic parameters are summarized in Table 15-SI.

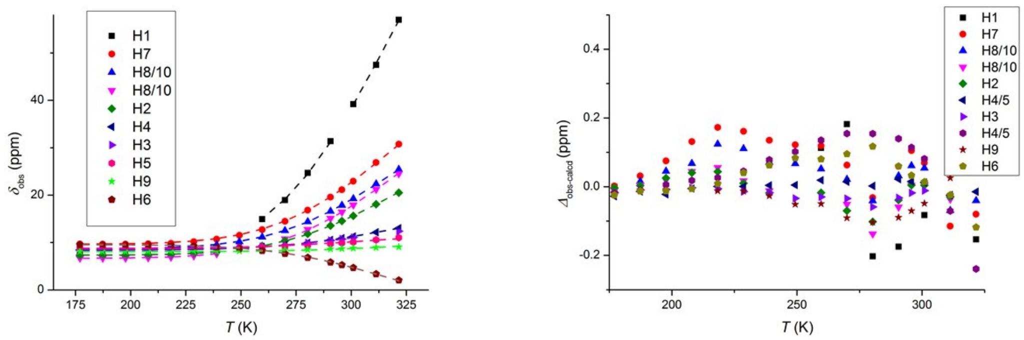

Figure 16-SI: left) Experimental (points) and calculated (dashed lines) chemical shifts of [Fe(**5c**)$_2$]$^{2+}$ recorded in d_6-acetone $\Delta_{SCO}H$ = 28.15 kJ/mol and $\Delta_{SCO}S$ = 81.5 J/(mol·K). right) residuals for the refinement. Refinement was done with fixed C^1 and δ_{dia} values.

Table 13-SI: NMR parameters extracted from refinement of ^{1}H chemical shifts of [Fe(**5c**)$_2$]$^{2+}$ recorded in d_6-acetone ΔH = 28.15 kJ/mol and ΔS = 81.5 J/(mol·K).

[Fe(**5c**)$_2$]$^{2+}$	C^0 (ppm K)	C^1 (ppm)	δ_{dia} (ppm)
H1	71418.47	-70.23	7.33
H7	26410.01	-17.69	9.67
H10/H8	21290.92	-14.90	8.68
H10/H8	19083.70	-4.30	6.69
H2	14175.61	-3.40	7.34
H4	4964.58	-1.35	8.42
H3	5974.01	-6.47	8.50
H5	5272.50	-10.26	8.79
H9	-755.59	5.83	8.11
H6	-10033.46	7.92	9.53

d_5-nitrobenzene solution

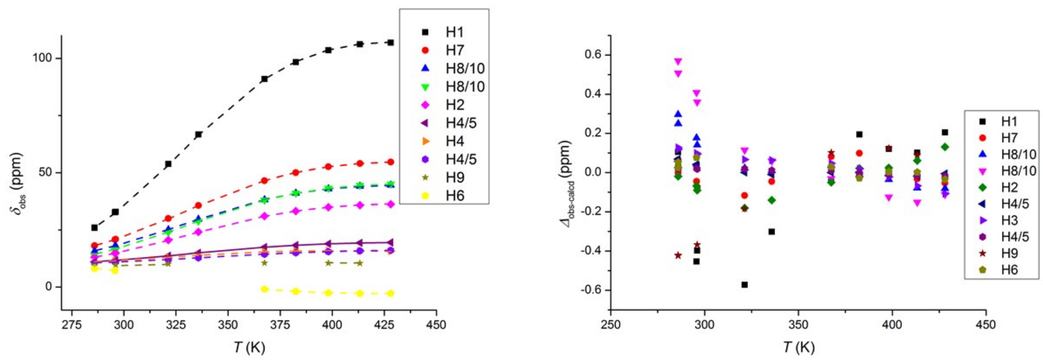

Figure 17-SI: left) Experimental (points) and calculated (dashed lines) chemical shifts of [Fe(**5c**)$_2$]$^{2+}$ recorded in d_5-nitrobenzene ($\Delta_{SCO}H$ = 28.15 kJ/mol and $\Delta_{SCO}S$ = 79 J/(mol·K)). right) residuals of the refinement. Refinement was done with fixed C^1 and δ_{dia} values.

Table 14-SI: NMR parameters extracted from refinement of chemical shifts of [Fe(**5c**)$_2$]$^{2+}$ recorded in d_5-nitrobenzene ($\Delta_{SCO}H$ = 28.15 kJ/mol and $\Delta_{SCO}S$ = 79 J/(mol·K)).

[Fe(**5c**)$_2$]$^{2+}$	C^0 (ppm K)	C^1 (ppm)	δ_{dia} (ppm)
H1	65777.22	-35.59	8.97
H7	25491.96	-6.88	10.87
H10/H8	20344.43	-6.30	10.22
H10/H8	20280.14	-3.46	8.46
H2	14787.87	-1.22	8.68
H4	4946.81	0.43	9.55
H3	7405.83	-10.05	9.64
H5	1079.78	4.93	9.91
H9	3740.41	-6.66	8.64
H6	-10517.73	8.38	10.68

Table 15-SI: Summary of the thermodynamic parameters from chemical shifts of [Fe(**5c**)$_2$]$^{2+}$.

	[Fe(**5c**)$_2$]$^{2+}$ in d_6-acetone fixed δ_{dia}; C^1	[Fe(**5c**)$_2$]$^{2+}$ in d_5-nitrobenzene fixed δ_{dia}; C^1	[Fe(**5c**)$_2$]$^{2+}$ in d_5-nitrobenzene fixed δ_{dia}; C^1 = 0	[Fe(**5c**)$_2$]$^{2+}$ in d_5-nitrobenzene fixed δ_{dia} and freely refin. C^1
$\Delta_{SCO}H$ [J]	28150	28150	28750	28550
$\Delta_{SCO}S$ [J K^{-1} mol^{-1}]	81.5	79	82	81
$T_{1/2}$ [K]	345	356	351	352

2.3.6 Thermodynamics from NMR - ^{1}H NMR data reduction for [Fe(5a)$_2$]$^{2+}$ and [Fe(5b)$_2$]$^{2+}$

The refinement was performed according to our recently published methodology with fixed C^1, C^0 values, transferred from [Fe(**5d**)$_2$]$^{2+}$, and a fixed SCO entropy of $\Delta_{SCO}S$ = 80 J/(mol·K). The transition temperature was estimated as 600K. Figure 18-SI presents the spectra and graphical representation of the fit results.

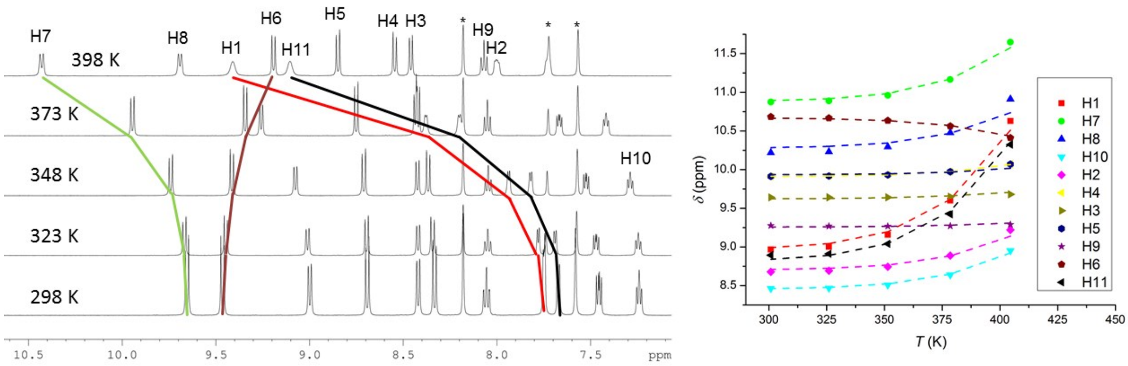

Figure 18-SI: left) VT ^{1}H-NMR spectra of [Fe(**5a**)$_2$]$^{2+}$ in d_5-nitrobenzene solution; right) graphical representation of observed and calculated chemical shifts; parameters used: $\Delta_{SCO}H$= 47.3 kJ/mol; $\Delta_{SCO}S$ = 80 J/(mol·K);

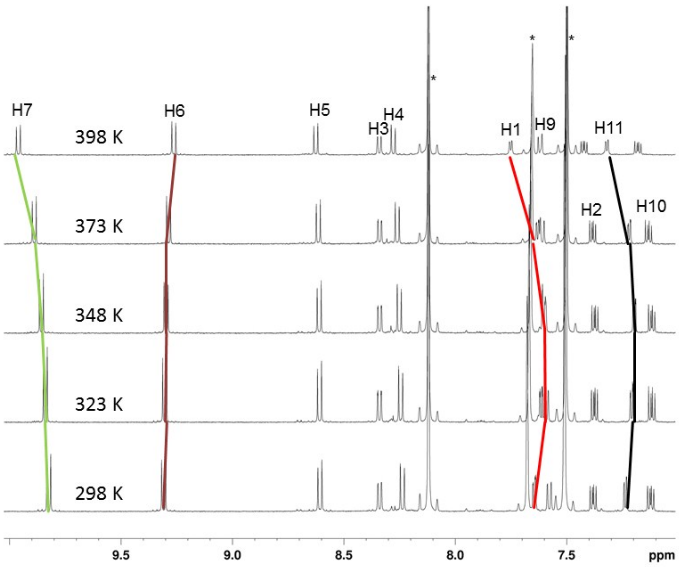

Figure 19-SI: VT ^{1}H NMR spectra of [Fe(**5b**)$_2$](BF$_4$)$_2$ in d_5-nitrobenzene solution.

2.3.7 Kinetics from NMR - [Fe(5c)$_2$]$^{2+}$

$$R_2 = \left\{(1-\gamma_{HS})R_{2(LS)} + \gamma_{HS}R_{2(HS)}\right\} + \left\{\gamma_{HS}(1-\gamma_{HS})\frac{\Delta\omega^2}{k_{ex}}\right\} \tag{4}$$

In order to determine the time constant for the SCO equilibrium of [Fe(**5c**)$_2$]$^{2+}$, the linewidths of *H*1 and *H*7 were used. The approach follows our recently published protocol using equation (4). The necessary R_2 times for the pure HS state were taken from [Fe(**5d**)$_2$]$^{2+}$ as a model for the pure HS form of [Fe(**5c**)$_2$]$^{2+}$. For d_5-nitrobenzene solution these values were taken without modification. The obtained kinetic data agree well with LFP experiments in acetonitrile solution (Figure 21-SI). However, the NMR method is obviously less accurate than the LFP experiment; therefore we refrain from extraction of activation barriers from ^{1}H NMR based data and just note the agreement. The origin of this deviation can be seen in the data recording paying attention to the chemical shifts rather than to the linewidths. Another problem is the validity of equation **(4)**, as such, for the fast exchange regime. With decreasing temperature this assumption is invalid as seen from studies on [Fe(**5d**)$_2$]$^{2+}$. Therefore we have used the exact treatment (McConnell equations) to recalculate the linewidths with the assumption of correct kinetics from the LFP experiment. Indeed the obvious deviation below 230 K results from the non-validity of equation (**4**). Figure 22-SI gives a graphical representation of the calculated linewidths.

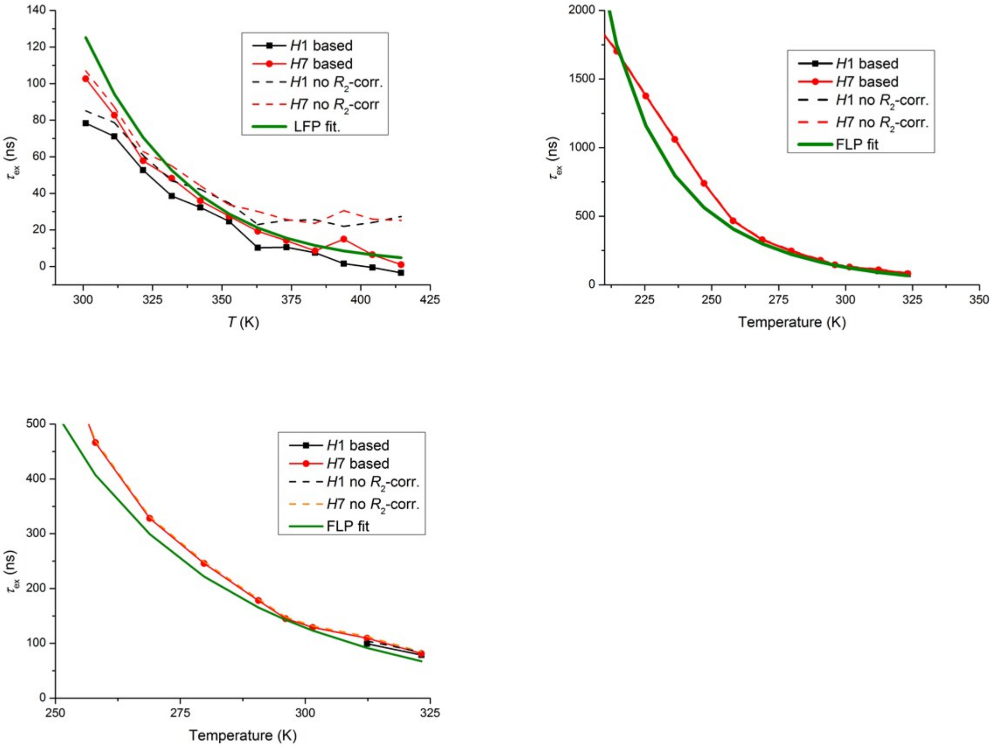

Figure 20-SI: Plot of the calculated time constant τ_{ex} from [1]H-NMR for proton *H*1 and *H*7 of $(Fe(\mathbf{5c})_2]^{2+}$ (d_5-nitrobenzene and d_6-acetone) and the kinetics obtained by fitting of the LFP results (acetonitrile). Top left: Results from the d_5-nitrobenzene solution. Top right and left bottom: Results from d_6-acetone solution. Note that with decreasing temperature the HS fraction decreases and therefore the contribution of the HS state to R_2 decreases; for the d_6-acetone solution this contribution can even be neglected. Results ignoring R_2 of the HS state are given as dashed lines. They are almost completely covered by the solid line below 300 K.

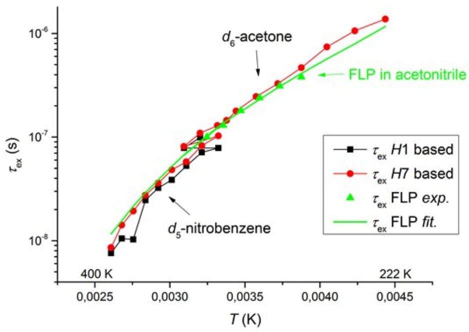

Figure 21-SI: Plot of the kinetic data obtained from LFP experiments (extrapolated) and [1]H NMR data refinement on $[Fe(\mathbf{5c})_2]^{2+}$

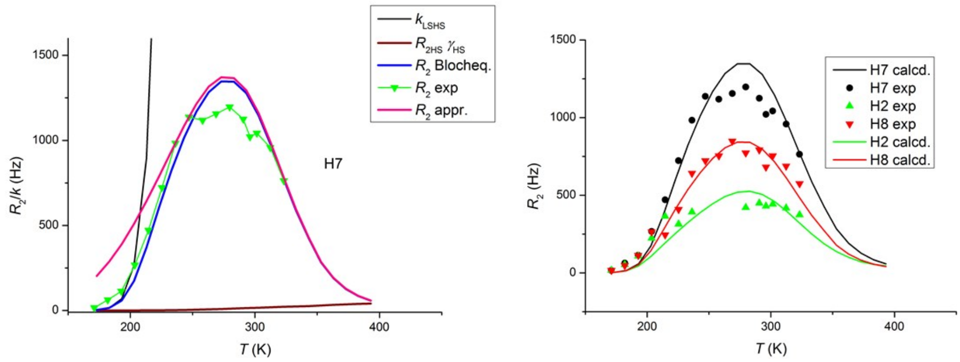

Figure 22-SI: left) graphical representation of the kinetic investigation using the approximation for fast exchange (4) (red line) and exact treatment (blue line) as an example using *H*7. For the calculation the kinetic parameters obtained from LFP, except $E_{a(HS\rightarrow LS)}$, and thermodynamic parameters obtained from NMR refinement were used ($\Delta_{SCO}H$ = 28.15 kJ/mol; $\Delta_{SCO}S$ = 81.5 J/(mol·K); C^0 = 79067 ppm·K; C^1 = -70 ppm; $E_{a(HS\rightarrow LS)}$ = 15.6 kJ/mol (15.0 from LFP); $A_{HS\rightarrow LS}$ = $2.66\cdot10^9$ s^{-1}; R_{2HS} from calculations on $[Fe(\mathbf{5d})_2]^{2+}$).

2.3.8 Simplified extraction of SCO lifetimes from NMR line widths

Irrespective of the inherent complexities, under favourable conditions a straightforward interpretation is possible. That is, at temperatures below the NMR-coalescence point of HS and LS species, the HS-state decay kinetics dominates the line widths of resonances associated to the HS species and *vice versa* the LS state decay dominates the linewidths of resonances associated to the LS species. Usually the coalescence temperatures for Fe^{2+} SCO complexes are such that only the major component, either HS or LS species, is observed in the ^{1}H NMR spectra. This statement reflects the variety of contributors to the transverse relaxation and, in the first place, their varying relevance in different temperature regimes. While in the absence of chemical exchange, the life time of the transversal magnetization -R_{2HS} or R_{2LS} for the pure states- ($t_{1/2}$/ln(2) = τ = "T_2" = 1/(π·LW); $t_{½}$ = half life time; τ = time constant) is dominated by the usual relaxation mechanism, chemical exchange in the fast-exchange limit can be accounted for by equation (4). Below the coalescence, however, the line widths are dominated by the life time of the species that causes the resonance, here HS or LS state with time constants $1/k_{HS\rightarrow LS}$ and $1/k_{LS\rightarrow HS}$, respectively.

As a rule of thumb, an equilibrium is well below the coalescence, if the time constant τ for the decay of the minor component of the equilibrium is << $2\pi/\Delta\omega$ = $\Delta(\delta_{HS}$-$\delta_{LS})(\omega_H)$ (ω_H is proton Larmor frequency, 2π·500 MHz in this case). Below the coalescence the chemical shift will return to the values of the individual components and the exchange broadening will be sharply reduced. These effects are well evident in the spectra of $[Fe(\mathbf{5d})_2]^{2+}$ at temperatures below 240 K. In this special situation the low temperature slope of the "SCO humps" in Figure 10-SI and Figure 23-SI carries the relaxation rates $k_{HS\rightarrow LS}$. The (approximated, see above) relaxivities R_2 of the pure HS state can be subtracted so that $k_{HS\rightarrow LS}$ can be read directly from the plots as is illustrated in Figure 23. It is worth to notice that this reading is independent of the mole fraction and hence also independent of the reverse reaction rate. These benefits render the *R_2-method* a very handy method to evaluate the life time of the HS state which can be seen as a solution equivalent of *T*(LIESST) an important parameter to characterize SCO complexes in solid state.[36] By way of extension of the method, also the rate constant for the relaxation from the LS to HS state of $[Fe(\mathbf{5c})_2]^{2+}$ (Figure 22-SI, left) can be read from the line widths. In this case the coalescence for *H*7 occurs at considerable lower temperatures

(<200 K) due to the lower activation barrier from the HS to the LS state. Again, below the coalescence the line width (LW) is the result of an exchange rate. At variance in this case it is the transformation of the LS to the HS state $k_{LS\rightarrow HS}$ ($k_{LS\rightarrow HS}$ = LW·π) (Figure 22-SI, right, blue and black line).[37]

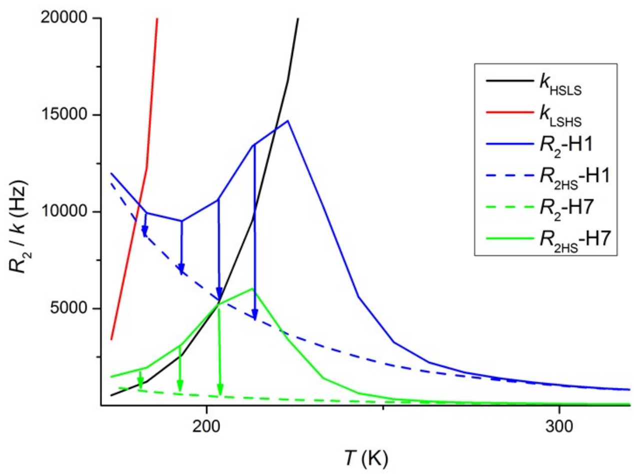

Figure 23-SI: Calculated line widths and reaction rates for protons *H*7 and *H*1 in [Fe(**5d**)$_2$]$^{2+}$ for d_6-acetone solution on the 500 MHz NMR; thermodynamic and kinetic parameters according to the text. The dashed lines give the R_2 values excluding exchange broadening and the lengths of the arrows are the reading for $k_{HS\rightarrow LS}$.

2.3.9 LIESST demonstration experiment

The SCO complex [Fe(**5d**)$_2$]$^{2+}$ is exceptional in that it combines a relatively slow SCO equilibration with and intensive MLCT band of the LS state. It is well known that such MLCT bands can be used to excite the LS state into the metastable HS state. The larger the absorption coefficient the less intensive light (photons per area) is needed to switch a significant amount of the complexes to the metastable HS state. In addition, complex [Fe(**5d**)$_2$]$^{2+}$ has a very low $T_{1/2}$ close to the theoretical limit, therefore a relative high T_{LIESST} is expected. Indeed at liquid nitrogen temperatures the metastable exited state is observable for several minutes. This allows an easy demonstration of the LIESST effect.

For this demonstration experiment an acetonitrile solution containing the complex [Fe(**5d**)$_2$](BF)$_2$ and Poly(ethyl methacrylate) (1:5 by mass) was dropped onto a filter paper After evaporation of the solvent, the dyed filter paper was dipped into liquid nitrogen and then removed. As long as the filter paper is soaked with liquid nitrogen, it is possible to write on the filter paper using a laser pointer (532nm, 10mW). The experiment is shown on the video found as supplementary information to this publication. Although this experiment will likely work with a number of similar complexes, to the best of our knowledge it has never been demonstrated before.

2.4 UV/vis electronic spectra

Electronic spectra were recorded using a Thermos electron corporation Genesys 6 spectrometer with quartz cuvettes (*d* = 0.01 m) with sample concentrations of c ≈ 1 mM and c ≈ 0.1 mM in spectroscopic grade acetonitrile.

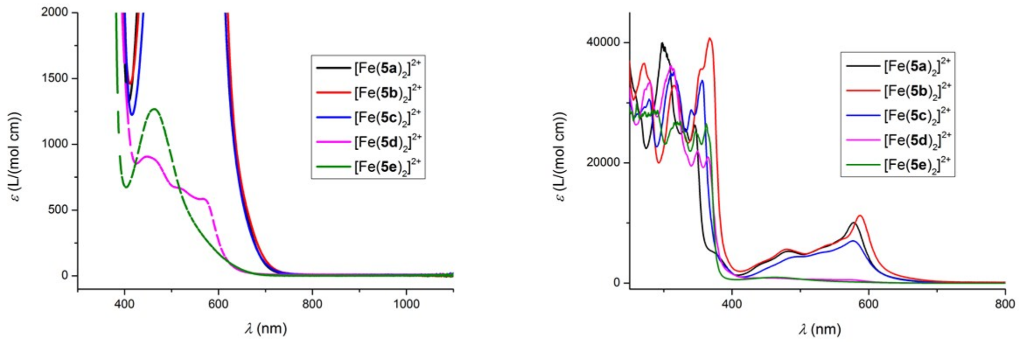

Figure 24-SI: Electronic spectra recorded in acetonitrile solution; left) c ≈ 1mM and right) c ≈ 0.1mM.

2.5 Literature

1 J. J. Moore, J. J. Nash, P. E. Fanwick and D. R. McMillin, *Inorg. Chem.*, 2002, **41**, 6387–6396.

2 F. Barigelletti, B. Ventura, J.-P. Collin, R. Kayhanian, P. Gavina and J.-P. Sauvage, *Eur. J. Inorg. Chem.*, 2000, 113–119.

3 R. Zong, D. Wang, R. Hammitt and R. P. Thummel, *J. Org. Chem.*, 2006, **71**, 167–175.

4 B. Paul, K. Chakrabarti, S. Shee, M. Maji, A. Mishra and S. Kundu, *RSC Adv.*, 2016, **6**, 100532–100545.

5 B. Paul, K. Chakrabarti and S. Kundu, *Dalt. Trans.*, 2016, **45**, 11162–11171.

6 F. Neese, *Wiley Interdiscip. Rev. Comput. Mol. Sci.*, 2012, **2**, 73–78.

7 A. Schäfer, H. Horn and R. Ahlrichs, *J. Chem. Phys.*, 1992, **97**, 2571–2577.

8 A. D. Becke, *J. Chem. Phys.*, 1993, **98**, 5648–5652.

9 C. Lee, W. Yang and R. G. Parr, *Phys. Rev. B*, 1988, **37**, 785–789.

10 S. Grimme, *J. Comput. Chem.*, 2006, **27**, 1787–1799.

11 K. Lagarec and D. G. Rancourt, 1998.

12 R. J. LeSuer, C. Buttolph and W. E. Geiger, *Anal. Chem.*, 2004, **76**, 6395–401.

13 F. Barrière, N. Camire, W. E. Geiger, U. T. Mueller-Westerhoff and R. Sanders, *J. Am. Chem. Soc.*, 2002, **124**, 7262–7263.

14 F. Barrière and W. E. Geiger, *J. Am. Chem. Soc.*, 2006, **128**, 3980–3989.

15 G. Gritzner and J. Kuta, *Pure Appl. Chem.*, 1984, **56**, 461–466.

16 A. Nafady and W. E. Geiger, *Organometallics*, 2008, **27**, 5624–5631.

17 I. Noviandri, K. N. Brown, D. S. Fleming, P. T. Gulyas, P. A. Lay, A. F. Masters and L. Phillips, *J. Phys. Chem. B*, 1999, **103**, 6713–6722.

18 G. M. Sheldrick, *Acta Cryst.*, 2008, **A24**, 112–122.

19 S. Alvarez, *Chem. Rev.*, 2015, **115**, 13447–13483.

20 S. Alvarez, P. Alemany, D. Casanova, J. Cirera, M. Llunell and D. Avnir, *Coord. Chem. Rev.*, 2005, **249**, 1693–1708.

21 David Avnir, *CSM page*, 2016, http://chirality.ch.huji.ac.il/new/?cmd=shape.26.

22 J. Conradie, A. K. Patra, T. C. Harrop and A. Ghosh, *Inorg. Chem.*, 2015, **54**, 1375–1383.

23 R. Adam, R. Ballesteros-Garrido, S. Ferrer, B. Abarca, R. Ballesteros, J. A. Real and M. C. Muñoz, *CrystEngComm*, 2016, **18**, 7950–7954.

24 E. L. Muetterties and L. J. Guggenberger, *J. Am. Chem. Soc.*, 1974, **96**, 1748–1756.

25 T. Pedzinski, A. Markiewicz and B. Marciniak, *Res. Chem. Intermed.*, 2009, **35**, 497–506.

26 A. L. Van Geet, *Anal. Chem.*, 1970, **42**, 3–4.

27 H. Petzold, P. Djomgoue, G. Hörner, J. M. Speck, T. Rüffer and D. Schaarschmidt, *Dalt. Trans.*, 2016, **45**, 13798–13809.

28 H. Petzold, *NMR_2SCO*, 2016, https://www.tu-chemnitz.de/chemie/anorg/hpetzold/forschung.php

29 H. F. G. Schilling, *Org. Magn. Reson.*, 1979, **12**, 569–573.

30 G. P. I. Bertini C. Luchinat, *Solution NMR of Paramagnetic Molecules*, Elsevier, 2001.

31 J. K. McCusker, A. L. Rheingold and D. N. Hendrickson, *Inorg. Chem.*, 1996, **35**, 2100–2112.

32 P. Stock, T. Pędziński, N. Spintig, A. Grohmann and G. Hörner, *Chem. - A Eur. J.*, 2013, **19**, 839–42.

33 G. Marius Clore and J. Iwahara, *Chem. Rev.*, 2009, **109**, 4108–4139.

34 A. D. Bain, *Prog. Nucl. Magn. Reson. Spectrosc.*, 2003, **43**, 63–103.

35 A. . McLaughlin and J. . Leigh, *J. Magn. Reson.*, 1973, **9**, 296–304.

36 J.-F. Letard, *J. Mater. Chem.*, 2006, **16**, 2550–2559.

37 L. Schnaubelt, H. Petzold, J. M. Speck, E. Dmitrieva, M. Rosenkranz and M. Korb, *Dalt. Trans.*, 2017, **46**, 2690–2698.

2.6 Cartesian coordinates of DFT optimized structures

Table 16-SI: Cartesian coordinates of the optimized structure of LS $[Fe(\mathbf{5a})_2]^{2+}$ (B3LYP*-D/TZVP).

C	7.024514	0.514427	4.563977
H	6.488232	0.559361	3.623397
C	6.516376	-0.218925	5.650521
H	5.576797	-0.743769	5.534828
C	7.208875	-0.261570	6.844609
H	6.821415	-0.817608	7.690954
C	8.431962	0.433339	6.951086
C	8.857370	1.132725	5.808894
C	9.262138	0.489531	8.123249
H	8.934318	-0.044503	9.007636
C	10.435239	1.192472	8.148177
H	11.036320	1.216945	9.049835
C	10.890436	1.904332	6.990603
C	10.078549	1.851262	5.846559
C	12.077426	2.667058	6.873005
H	12.752503	2.743724	7.717908
C	12.375886	3.318297	5.687501
H	13.282831	3.902468	5.600461
C	11.491746	3.220959	4.594596
C	11.587325	3.840957	3.268716
C	12.633998	4.647682	2.837495
H	13.457258	4.867811	3.505096
C	12.606547	5.163651	1.546285
H	13.413214	5.792298	1.189276
C	11.530092	4.857204	0.721592
H	11.469692	5.238672	-0.289505
C	10.511443	4.051466	1.217128
H	9.651479	3.793999	0.611023
C	8.109589	4.869737	4.786915
H	8.962257	4.758671	5.446146
C	7.183288	5.910322	4.974760
H	7.335210	6.603928	5.792135
C	6.099347	6.037955	4.128558
H	5.377102	6.834280	4.269143
C	5.944687	5.114289	3.073899
C	6.925472	4.112968	2.966855
C	4.873006	5.114501	2.115272
H	4.113684	5.883947	2.197829
C	4.789831	4.178954	1.121626
H	3.964540	4.204592	0.419444
C	5.784244	3.155405	0.990719
C	6.835124	3.159538	1.921546
C	5.822399	2.127807	0.017636
H	5.037527	2.064270	-0.727548
C	6.853416	1.203268	0.015805
H	6.874748	0.413444	-0.724643
C	7.872324	1.291133	0.985964
C	9.042734	0.428930	1.182385
C	9.396739	-0.633721	0.360261
H	8.787291	-0.875326	-0.501284
C	10.539372	-1.370579	0.654869
H	10.834742	-2.200122	0.023997
C	11.294747	-1.023352	1.769456
H	12.189346	-1.570901	2.036705
C	10.888661	0.054573	2.547644
H	11.451461	0.364007	3.420073
N	8.166655	1.189165	4.632731
N	10.382747	2.487261	4.703665
N	10.526831	3.549557	2.455972
N	7.992067	3.978009	3.808447
N	7.832788	2.260648	1.901561
N	9.794762	0.771447	2.272108
Fe	9.126793	2.370416	3.286094

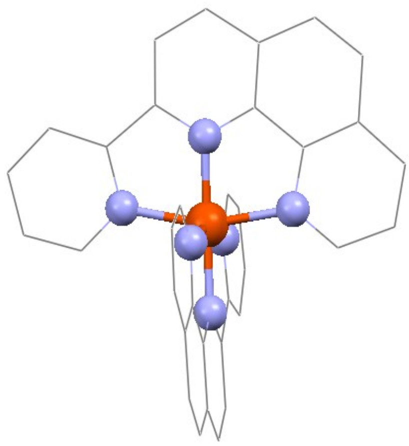

Table 17-SI: Cartesian coordinates of the optimized structure of HS $[Fe(\mathbf{5a})_2]^{2+}$ (B3LYP*-D/TZVP).

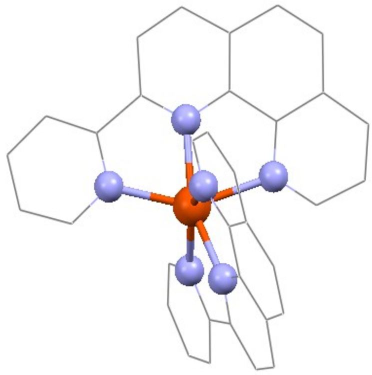

C	7.296226	0.272256	4.471152
H	6.938599	0.098292	3.461684
C	6.646118	-0.319863	5.567851
H	5.787357	-0.956861	5.398925
C	7.109553	-0.073487	6.842683
H	6.623795	-0.510905	7.707797
C	8.234423	0.758641	7.016206
C	8.821770	1.295443	5.850774
C	8.799375	1.076343	8.296016
H	8.330970	0.658832	9.180215
C	9.898517	1.874388	8.409321
H	10.316766	2.104250	9.382453
C	10.527618	2.419038	7.245622
C	9.980068	2.129452	5.976362
C	11.678603	3.235046	7.261985
H	12.143433	3.483487	8.209767
C	12.212640	3.714634	6.082347
H	13.096175	4.338071	6.098597
C	11.590753	3.386228	4.862364
C	12.033907	3.840145	3.525550
C	13.196015	4.574415	3.311742
H	13.827450	4.856722	4.143449
C	13.540866	4.934325	2.012553
H	14.444746	5.501028	1.825034
C	12.713838	4.552184	0.963282
H	12.949556	4.812257	-0.060815
C	11.564336	3.823830	1.255783
H	10.888595	3.506686	0.468531
C	8.283406	4.988346	4.522764
H	9.263112	5.014778	4.987042
C	7.304267	5.932440	4.875977
H	7.537076	6.691419	5.612101
C	6.063337	5.873996	4.279018
H	5.285806	6.584058	4.538349
C	5.809237	4.874415	3.317305
C	6.861539	3.979294	3.027023
C	4.555920	4.722821	2.636096
H	3.756088	5.415311	2.873627
C	4.362672	3.739581	1.712029
H	3.408396	3.637449	1.208112
C	5.412950	2.825018	1.387275
C	6.655691	2.956274	2.044968
C	5.306576	1.779602	0.445422
H	4.370732	1.627896	-0.081117
C	6.383221	0.952655	0.195687
H	6.297950	0.152535	-0.526996
C	7.588384	1.162718	0.892656
C	8.822168	0.366232	0.719088
C	8.964950	-0.619875	-0.252315
H	8.146363	-0.859308	-0.917881
C	10.180943	-1.286457	-0.367700
H	10.315422	-2.052081	-1.122181
C	11.217987	-0.949157	0.493341
H	12.181416	-1.438825	0.431053
C	10.995826	0.039227	1.448298
H	11.776833	0.328492	2.143200
N	8.351613	1.063046	4.600210
N	10.509673	2.612193	4.841926
N	11.228633	3.474087	2.500059
N	8.075057	4.032580	3.628742
N	7.689938	2.139925	1.788893
N	9.831750	0.683931	1.563855
Fe	9.422506	2.303800	3.028492

Table 18-SI: Cartesian coordinates of the optimized structure of LS $[Fe(\mathbf{5b})_2]^{2+}$ (B3LYP*-D/TZVP).

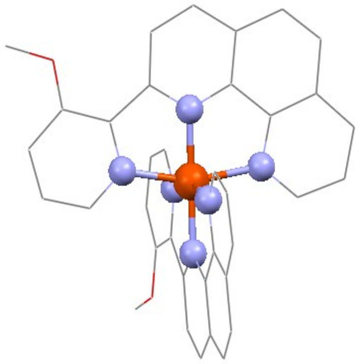

C	7.043985	0.600909	4.300173
H	6.541327	0.730024	3.347738
C	6.492114	-0.208114	5.309567
H	5.549880	-0.710113	5.124620
C	7.146358	-0.354888	6.518428
H	6.727219	-0.974193	7.305092
C	8.375315	0.309986	6.718394
C	8.848284	1.090720	5.648134
C	9.169523	0.255358	7.917158
H	8.803154	-0.338655	8.747923
C	10.359597	0.920906	8.027077
H	10.936642	0.857851	8.943735
C	10.870270	1.702824	6.937715
C	10.094509	1.760421	5.767987
C	12.086429	2.425431	6.903439
H	12.732984	2.430965	7.775160
C	12.460736	3.127712	5.768850
H	13.390678	3.675401	5.742598
C	11.618223	3.131130	4.632675
C	11.776504	3.803019	3.335999
C	12.907467	4.537991	2.914357
H	13.729270	5.715340	1.298703
C	12.882312	5.139484	1.649579
O	13.946420	4.604043	3.760913
C	11.762407	4.986768	0.846690
H	11.720924	5.446559	-0.133591
C	10.687472	4.233829	1.305424
H	9.800045	4.078813	0.704966
C	8.176358	4.839742	4.892721
H	8.996557	4.655289	5.577997
C	7.236538	5.857007	5.140508
H	7.341530	6.463633	6.032411
C	6.197117	6.072544	4.255170
H	5.464972	6.852553	4.439659
C	6.093881	5.259007	3.106239
C	7.081743	4.269899	2.946183
C	5.059504	5.349818	2.109631
H	4.299283	6.114992	2.229241
C	5.012548	4.501579	1.037841
H	4.214585	4.590442	0.307555
C	6.001499	3.476405	0.866338
C	7.025817	3.401050	1.824810
C	6.056271	2.514568	-0.169308
H	5.299259	2.518694	-0.947428
C	7.058809	1.558060	-0.193924
H	7.091579	0.817728	-0.978890
C	8.046549	1.546077	0.820073
C	9.175120	0.630738	1.035919
C	9.529745	-0.460125	0.211985
H	10.948002	-2.069329	-0.057945
C	10.649285	-1.228994	0.555935
O	8.754446	-0.690899	-0.857378
C	11.370993	-0.903768	1.694164
H	12.239539	-1.484923	1.981345
C	10.972673	0.176896	2.472206
H	11.507535	0.463813	3.368943
N	8.197282	1.244481	4.456445
N	10.461125	2.455733	4.678107
N	10.696415	3.654618	2.509995
N	8.109449	4.054103	3.820983
N	8.000335	2.475414	1.785013
N	9.906940	0.918347	2.154873
Fe	9.239341	2.474046	3.224314
C	15.144401	5.298917	3.352032
H	15.844143	5.177436	4.177797
H	14.933709	6.360331	3.186957
H	15.554503	4.845068	2.444282
C	9.059117	-1.807555	-1.718756
H	8.979288	-2.746297	-1.161057
H	10.061014	-1.698359	-2.145961
H	8.312036	-1.775880	-2.510265

Table 19-SI: Cartesian coordinates of the optimized structure of HS $[Fe(\mathbf{5b})_2]^{2+}$ (B3LYP*-D/TZVP).

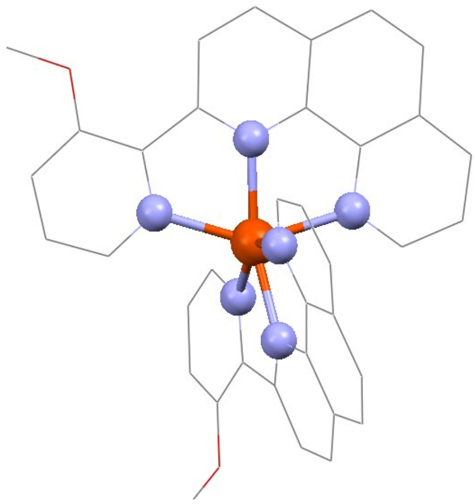

C	7.161572	0.366531	4.585208
H	6.768530	0.226167	3.582915
C	6.519999	-0.214257	5.693348
H	5.629069	-0.812206	5.541527
C	7.031238	-0.004692	6.957627
H	6.551029	-0.432839	7.831612
C	8.200396	0.771074	7.109306
C	8.778399	1.296588	5.933092
C	8.815132	1.051744	8.376165
H	8.350655	0.652634	9.272033
C	9.958143	1.790350	8.462308
H	10.411835	1.995140	9.426419
C	10.587772	2.306385	7.283953
C	9.991971	2.056156	6.027990
C	11.785792	3.051118	7.268202
H	12.279486	3.287688	8.205588
C	12.337258	3.477226	6.074977
H	13.261847	4.033956	6.060626
C	11.675659	3.180960	4.863539
C	12.099383	3.592723	3.504818
C	13.408376	3.989304	3.147067
H	14.630202	4.712685	1.516561
C	13.644807	4.383999	1.822057
O	14.359652	3.937954	4.094294
C	12.605774	4.357764	0.905263
H	12.764307	4.677237	-0.118198
C	11.355411	3.904692	1.314076
H	10.521604	3.836663	0.623295
C	8.179665	4.992924	4.570385
H	9.148399	5.008322	5.060290
C	7.203108	5.954956	4.881394
H	7.422567	6.719337	5.617912
C	5.981124	5.910906	4.241461
H	5.208817	6.640641	4.464653
C	5.739424	4.902913	3.283953
C	6.782551	3.981082	3.044326
C	4.505525	4.764664	2.562327
H	3.711424	5.477155	2.762145
C	4.326374	3.771481	1.645181
H	3.387100	3.678158	1.109891
C	5.369483	2.829826	1.371642
C	6.595812	2.951481	2.062811
C	5.280858	1.771717	0.444132
H	4.362291	1.627205	-0.116238
C	6.349830	0.919288	0.239085
H	6.281495	0.112285	-0.473525
C	7.543663	1.115876	0.968915
C	8.799732	0.335333	0.848830
C	9.008120	-0.764339	-0.017877
H	10.497254	-2.133784	-0.779261
C	10.298554	-1.308394	-0.107648
O	7.958569	-1.236261	-0.707744
C	11.320292	-0.785487	0.666535
H	12.323518	-1.190391	0.602376
C	11.034610	0.261199	1.538461
H	11.793464	0.692951	2.182555
N	8.258557	1.104780	4.693852
N	10.526121	2.500493	4.877867
N	11.121352	3.527215	2.571800
N	7.981764	4.028265	3.679493
N	7.625473	2.116479	1.851360
N	9.815569	0.793189	1.618565
Fe	9.326880	2.336339	3.121372
C	15.736674	4.151911	3.715838
H	16.317846	3.950395	4.614169
H	15.889501	5.185230	3.389093
H	16.022557	3.456410	2.920475
C	8.149286	-2.359487	-1.594188
H	8.507315	-3.228229	-1.032789
H	8.853911	-2.100077	-2.390297
H	7.167947	-2.565291	-2.018128

Table 20-SI: Cartesian coordinates of the optimized structure of LS $[Fe(\mathbf{5c})_2]^{2+}$ (B3LYP*-D/TZVP).

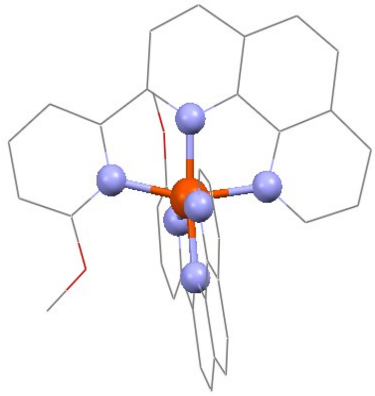

C	6.732305	0.484079	4.651714
H	6.251449	0.510577	3.681423
C	6.153819	-0.219379	5.721930
H	5.217205	-0.738092	5.562842
C	6.773822	-0.238880	6.955352
H	6.332090	-0.769868	7.791067
C	7.995557	0.445697	7.116538
C	8.496141	1.114743	5.986238
C	8.754357	0.519162	8.334508
H	8.366971	0.010587	9.209856
C	9.933164	1.207144	8.410534
H	10.481262	1.247243	9.344808
C	10.466088	1.883027	7.264820
C	9.721672	1.819222	6.075625
C	11.670464	2.622426	7.204832
H	12.293019	2.709299	8.088082
C	12.047788	3.238971	6.025028
H	12.966173	3.809190	5.978843
C	11.226792	3.130574	4.884425
C	11.439797	3.709962	3.556212
C	12.573183	4.421981	3.200673
H	13.353703	4.604175	3.926516
C	12.683160	4.886942	1.892975
H	13.558727	5.441684	1.578211
C	11.668043	4.631915	0.989282
H	11.738005	4.983708	-0.029450
C	10.538862	3.918219	1.422933
O	9.498093	3.623050	0.638384
C	8.057879	4.835836	5.025192
H	8.963791	4.712564	5.605695
C	7.162902	5.883847	5.297654
H	7.397508	6.576520	6.096094
C	6.002449	6.017597	4.560121
H	5.300136	6.816020	4.771730
C	5.741748	5.094903	3.525580
C	6.704733	4.091771	3.320184
C	4.579592	5.094390	2.679270
H	3.831776	5.863344	2.836312
C	4.398319	4.155602	1.702029
H	3.505316	4.177331	1.088314
C	5.377338	3.135012	1.469276
C	6.518705	3.141134	2.286483
C	5.315863	2.106406	0.499058
H	4.456626	2.037557	-0.158369
C	6.344109	1.186112	0.394839
H	6.292387	0.394194	-0.341505
C	7.457224	1.279218	1.255015
C	8.648285	0.427067	1.300151
C	8.920465	-0.573487	0.381150
H	8.216387	-0.796526	-0.408803
C	10.123529	-1.267344	0.490995
H	10.370003	-2.052563	-0.213502
C	11.014065	-0.940619	1.498268
H	11.955169	-1.461725	1.593937
C	10.666265	0.074586	2.403131
O	11.441135	0.472963	3.416482
N	7.875420	1.151258	4.772273
N	10.101347	2.423567	4.939032
N	10.420304	3.465042	2.678660
N	7.841473	3.947043	4.061088
N	7.512408	2.247089	2.166024
N	9.508387	0.743195	2.315041
Fe	8.895504	2.326952	3.469642
C	9.500122	4.088839	-0.722176
C	12.771380	-0.058547	3.535815
H	12.745640	-1.133188	3.737302
H	13.217031	0.466145	4.378710
H	13.343022	0.140923	2.624858
H	10.342210	3.661224	-1.272209
H	8.562131	3.738956	-1.148836
H	9.544061	5.181049	-0.755186

Table 21-SI: Cartesian coordinates of the optimized structure of HS $[Fe(\mathbf{5c})_2]^{2+}$ (B3LYP*-D/TZVP).

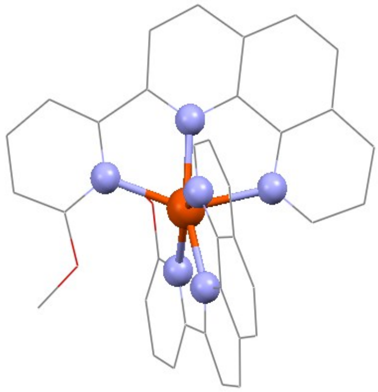

C	7.040106	0.399401	4.616296
H	6.671704	0.244426	3.607617
C	6.372261	-0.172103	5.713123
H	5.485979	-0.770868	5.545987
C	6.855094	0.044610	6.985979
H	6.358105	-0.379168	7.851426
C	8.016735	0.824839	7.156990
C	8.614761	1.350365	5.991426
C	8.609945	1.099277	8.433586
H	8.132119	0.693382	9.318108
C	9.749488	1.839105	8.543650
H	10.190291	2.032386	9.514796
C	10.390770	2.369124	7.379773
C	9.808430	2.133720	6.114565
C	11.586122	3.118856	7.392273
H	12.074894	3.327265	8.337580
C	12.133275	3.580706	6.211839
H	13.051617	4.152004	6.222071
C	11.472471	3.313280	4.997138
C	11.935073	3.745408	3.660008
C	13.191630	4.280433	3.423626
H	13.890172	4.435713	4.234029
C	13.538128	4.601564	2.110627
H	14.514654	5.016185	1.891459
C	12.635116	4.389400	1.083926
H	12.890063	4.635883	0.063116
C	11.380444	3.848955	1.409844
O	10.414538	3.577501	0.521857
C	8.053525	5.021455	4.689950
H	9.032420	5.058599	5.156180
C	7.056645	5.943770	5.052063
H	7.273935	6.696800	5.798985
C	5.818617	5.870912	4.450366
H	5.027898	6.563851	4.716137
C	5.584792	4.878773	3.475629
C	6.652640	4.004556	3.179268
C	4.336997	4.714134	2.787276
H	3.524739	5.390072	3.030378
C	4.163837	3.739234	1.850078
H	3.213283	3.628273	1.341116
C	5.229795	2.845009	1.519242
C	6.466162	2.987312	2.186425
C	5.146608	1.808825	0.564098
H	4.216461	1.648912	0.029988
C	6.237789	1.001433	0.312116
H	6.171432	0.207788	-0.419846
C	7.433008	1.218314	1.024765
C	8.680923	0.442218	0.858447
C	8.874416	-0.498957	-0.141644
H	8.086106	-0.738327	-0.841762
C	10.121642	-1.117885	-0.234036
H	10.308803	-1.850900	-1.009551
C	11.126956	-0.791823	0.660879
H	12.099133	-1.258670	0.596566
C	10.840382	0.155462	1.657317
O	11.701039	0.567303	2.599288
N	8.127032	1.145958	4.743495
N	10.341389	2.615818	4.981646
N	11.047615	3.537425	2.661516
N	7.863643	4.072959	3.784535
N	7.511120	2.186360	1.931941
N	9.652405	0.749783	1.746444
Fe	9.240227	2.376775	3.170718
C	10.634177	3.919976	-0.858716
H	10.800033	4.995400	-0.964355
H	9.725023	3.628345	-1.380179
H	11.488118	3.367839	-1.259423
C	13.051939	0.079024	2.570353
H	13.076190	-1.001955	2.735732
H	13.564690	0.591199	3.381505
H	13.525366	0.325501	1.615243

Table 22-SI: Cartesian coordinates of the optimized structure of LS $[Fe(\mathbf{5d})_2]^{2+}$ (B3LYP*-D/TZVP).

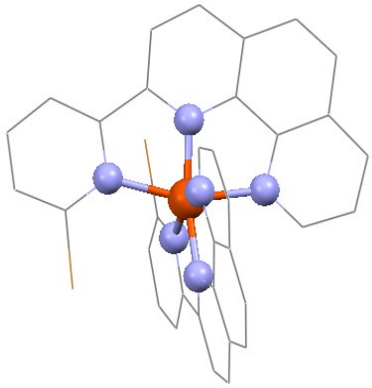

C	6.894624	0.354356	4.532352
H	6.455589	0.320098	3.543227
C	6.301150	-0.340699	5.599594
H	5.402345	-0.915110	5.415497
C	6.853267	-0.273331	6.862845
H	6.394633	-0.788907	7.699073
C	8.028103	0.481188	7.053658
C	8.559000	1.121709	5.920074
C	8.705842	0.654752	8.308280
H	8.292731	0.167982	9.184390
C	9.836602	1.414178	8.415919
H	10.322510	1.538359	9.376845
C	10.399982	2.060635	7.268659
C	9.744802	1.886676	6.038181
C	11.550262	2.882155	7.251312
H	12.103696	3.054061	8.167468
C	11.954913	3.480275	6.072823
H	12.825201	4.122458	6.063155
C	11.224310	3.257120	4.887853
C	11.482604	3.823782	3.563995
C	12.599809	4.596283	3.289357
H	13.303733	4.824934	4.077866
C	12.811333	5.050264	1.993233
H	13.682248	5.644858	1.746159
C	11.888792	4.720595	1.016502
H	12.012890	5.046747	-0.006920
C	10.772035	3.962236	1.376602
Br	9.527670	3.591382	-0.006443
C	8.190256	4.808169	4.974414
H	9.115886	4.697423	5.523852
C	7.300341	5.850061	5.282339
H	7.562558	6.544129	6.070910
C	6.110838	5.975493	4.592095
H	5.410532	6.768024	4.831037
C	5.816405	5.049257	3.570582
C	6.778955	4.054080	3.324054
C	4.616730	5.038874	2.779526
H	3.873125	5.805113	2.966727
C	4.395270	4.091671	1.819862
H	3.474755	4.101258	1.248011
C	5.368290	3.075218	1.551274
C	6.552531	3.096283	2.306118
C	5.254725	2.032734	0.602661
H	4.362194	1.953806	-0.007459
C	6.273836	1.109240	0.462886
H	6.180084	0.305075	-0.255041
C	7.434064	1.222564	1.255200
C	8.622312	0.370513	1.223606
C	8.795559	-0.631495	0.282021
H	8.015521	-0.835368	-0.438877
C	9.986906	-1.346896	0.261182
H	10.155570	-2.126912	-0.471234
C	10.964047	-1.035502	1.189824
H	11.911065	-1.556715	1.207705
C	10.705470	-0.028661	2.123598
Br	12.074758	0.319220	3.388067
N	7.994911	1.086105	4.679396
N	10.163677	2.455159	4.894745
N	10.542726	3.507110	2.610038
N	7.944571	3.916215	4.019351
N	7.546287	2.207991	2.140003
N	9.574600	0.677899	2.168362
Fe	8.995237	2.296694	3.386821

Table 23-SI: Cartesian coordinates of the optimized structure of HS $[Fe(\mathbf{5d})_2]^{2+}$ (B3LYP*-D/TZVP).

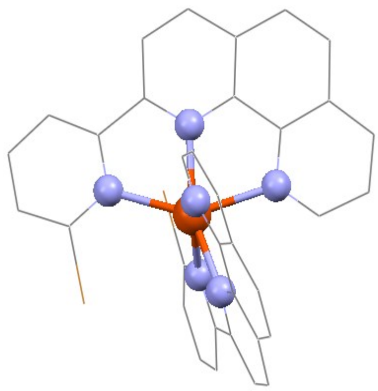

C	7.234054	0.238059	4.552089
H	6.891331	0.048689	3.540414
C	6.581676	-0.355573	5.646534
H	5.736877	-1.010123	5.474116
C	7.025409	-0.088295	6.923721
H	6.537051	-0.525503	7.787382
C	8.133508	0.764928	7.102073
C	8.724805	1.301611	5.938568
C	8.678363	1.102476	8.385109
H	8.205716	0.686843	9.267944
C	9.764835	1.916521	8.502492
H	10.169641	2.161144	9.477774
C	10.398167	2.460313	7.340751
C	9.866945	2.157148	6.067798
C	11.538263	3.290651	7.364940
H	11.990053	3.550524	8.315888
C	12.075762	3.771544	6.188376
H	12.948361	4.409876	6.210666
C	11.466224	3.433579	4.964238
C	11.918288	3.903789	3.638110
C	13.110826	4.585330	3.440275
H	13.759482	4.811538	4.275167
C	13.468816	4.962406	2.147722
H	14.400192	5.484848	1.966519
C	12.622204	4.663420	1.092440
H	12.860374	4.943928	0.075538
C	11.437744	3.987857	1.386747
Br	10.229446	3.593517	-0.030494
C	8.203989	5.003220	4.614334
H	9.185590	5.025273	5.074371
C	7.233753	5.955981	4.968183
H	7.475352	6.715573	5.700847
C	5.991041	5.905555	4.374842
H	5.220081	6.623318	4.632577
C	5.726015	4.904317	3.418061
C	6.768743	3.997258	3.129810
C	4.470368	4.765014	2.739379
H	3.678445	5.466798	2.975987
C	4.266905	3.783090	1.816976
H	3.312314	3.690869	1.312063
C	5.306755	2.855776	1.495230
C	6.550320	2.968947	2.155257
C	5.185689	1.813949	0.552056
H	4.248467	1.676527	0.024363
C	6.250619	0.973375	0.303184
H	6.154524	0.175571	-0.420298
C	7.456162	1.162764	1.005847
C	8.670796	0.343326	0.822217
C	8.801022	-0.605986	-0.182177
H	7.987146	-0.799832	-0.866979
C	10.005154	-1.294670	-0.310559
H	10.136328	-2.031214	-1.094019
C	11.038625	-1.027176	0.572886
H	11.990053	-1.536646	0.506650
C	10.812134	-0.068085	1.560540
Br	12.196199	0.310203	2.810049
N	8.272728	1.049630	4.685911
N	10.396393	2.646459	4.935370
N	11.089244	3.604249	2.604688
N	7.984596	4.045168	3.725625
N	7.571413	2.133537	1.905920
N	9.680397	0.605944	1.691016
Fe	9.321188	2.307607	3.120233

Table 24-SI: Cartesian coordinates of the optimized structure of LS [Fe(**5e**)$_2$]$^{2+}$ (B3LYP-0-D/TZVP).

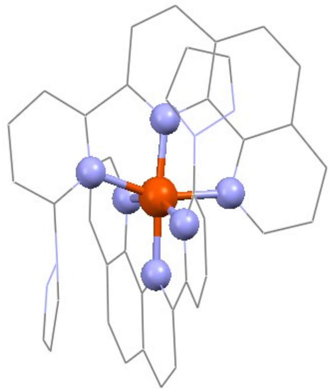

C	1.756963	1.869630	8.938375
H	0.860220	1.517510	9.447441
C	1.689615	2.426700	7.647168
H	0.718421	2.494725	7.157124
C	2.836593	2.886783	7.015342
H	2.788129	3.326502	6.018084
C	4.076274	2.772480	7.684295
C	4.048400	2.188894	8.968844
C	5.353992	3.196285	7.175055
H	5.388316	3.654942	6.185660
C	6.512922	3.036524	7.897380
H	7.464940	3.373437	7.484098
C	6.499203	2.423427	9.194843
C	5.247495	2.005435	9.686706
C	7.617148	2.171671	10.031605
H	8.614961	2.475680	9.712254
C	7.439280	1.534830	11.252165
H	8.293327	1.338720	11.900229
C	6.145240	1.144537	11.663536
C	5.735091	0.481532	12.891573
C	6.626296	-0.066985	13.813498
H	7.698024	0.043191	13.648758
C	6.133191	-0.765734	14.911442
H	6.808964	-1.205914	15.645204
C	4.752061	-0.871276	15.065207
H	4.304655	-1.367553	15.925758
C	3.911224	-0.279713	14.120670
C	1.767050	-1.479006	14.520125
H	2.175854	-2.464960	14.321913
C	0.526483	-1.060223	14.952029
H	-0.327823	-1.684048	15.194687
C	0.626319	0.351877	15.028537
H	-0.129010	1.066826	15.344572
C	4.089051	3.863808	12.349430
H	5.119061	3.597649	12.113358
C	3.761473	5.143340	12.836943
H	4.562120	5.868479	12.982164
C	2.443985	5.475187	13.120853
H	2.184421	6.467506	13.493280
C	1.438353	4.501720	12.926424
C	1.861444	3.245701	12.443093
C	0.031781	4.678555	13.173206
H	-0.309630	5.648286	13.539040
C	-0.875635	3.666819	12.963967
H	-1.936317	3.836269	13.157478
C	-0.452666	2.376839	12.498489
C	0.925570	2.206868	12.264995
C	-1.270972	1.240488	12.269751
H	-2.348910	1.306341	12.426470
C	-0.698091	0.045672	11.854517
H	-1.320423	-0.830878	11.677133
C	0.697852	-0.036231	11.653144
C	1.496262	-1.172701	11.220091
C	1.005649	-2.474461	11.121599
H	-0.047776	-2.664338	11.325604
C	1.874043	-3.510794	10.792544
H	1.515449	-4.537241	10.711334
C	3.210751	-3.204019	10.544808
H	3.929301	-3.963629	10.239610
C	3.636588	-1.877502	10.637789
C	6.097919	-2.153381	10.879063
H	6.033229	-2.763245	11.774949
C	7.165279	-1.769049	10.095571
H	8.209359	-2.028545	10.238679
C	6.592577	-0.987841	9.060156
H	7.090254	-0.508632	8.220859
N	2.914818	1.747369	9.599784
N	5.086142	1.380541	10.873912
N	4.364936	0.375536	13.030505
N	2.516994	-0.343680	14.330172
N	1.829208	0.794698	14.664107
N	3.160258	2.919866	12.151994
N	1.474110	1.037522	11.866819
N	2.821412	-0.859338	10.988178
N	4.979815	-1.580864	10.322846
N	5.270101	-0.876402	9.182574
Fe	3.311376	1.065166	11.434053

Table 25-SI: Cartesian coordinates of the optimized structure of HS $[Fe(\mathbf{5e})_2]^{2+}$ (B3LYP-0-D/TZVP).

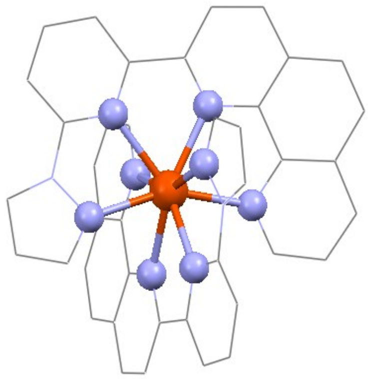

C	0.828317	0.426578	8.821967
H	0.392323	-0.103225	9.657634
C	0.116376	0.526997	7.616062
H	-0.861848	0.068200	7.533366
C	0.681537	1.204265	6.558029
H	0.164132	1.298754	5.608446
C	1.950013	1.793715	6.723838
C	2.583939	1.641363	7.982549
C	2.608326	2.519146	5.677229
H	2.105458	2.611643	4.720051
C	3.827755	3.089474	5.874174
H	4.318502	3.638056	5.077076
C	4.483683	2.982170	7.139845
C	3.859083	2.268295	8.196223
C	5.734490	3.568701	7.414205
H	6.250416	4.118499	6.633508
C	6.292332	3.438573	8.667091
H	7.256941	3.878717	8.885241
C	5.596934	2.713988	9.654381
C	6.117428	2.501816	11.019908
C	7.217480	3.174771	11.546340
H	7.758278	3.906451	10.960181
C	7.603155	2.896418	12.857459
H	8.446849	3.413479	13.300535
C	6.901966	1.957363	13.597047
H	7.187148	1.720390	14.613401
C	5.823233	1.322330	12.972963
C	5.316693	-0.300388	14.812162
H	6.127211	-0.003525	15.458469
C	4.369096	-1.282915	14.943591
H	4.250723	-1.968784	15.768330
C	3.593831	-1.199975	13.766519
H	2.745543	-1.802639	13.484414
C	3.157080	3.952404	11.680284
H	4.074003	4.005123	11.112226
C	2.623470	5.125318	12.236039
H	3.134301	6.068759	12.081638
C	1.459742	5.050905	12.968276
H	1.020670	5.933745	13.422085
C	0.831076	3.800600	13.123345
C	1.439522	2.677621	12.505577
C	-0.381956	3.639221	13.868693
H	-0.818118	4.515395	14.337372
C	-0.977397	2.422579	13.986609
H	-1.894979	2.305941	14.553206
C	-0.407340	1.272816	13.356455
C	0.791865	1.398702	12.605638
C	-0.986202	-0.007691	13.432448
H	-1.895056	-0.151866	14.007499
C	-0.396798	-1.063759	12.774149
H	-0.834799	-2.051951	12.831057
C	0.776536	-0.839828	12.026885
C	1.441889	-1.898179	11.238999
C	0.917260	-3.175655	11.057525
H	-0.023337	-3.464990	11.506565
C	1.622745	-4.079135	10.263192
H	1.231090	-5.075392	10.089986
C	2.824980	-3.700413	9.689536
H	3.389914	-4.387038	9.073301
C	3.274847	-2.399603	9.937849
C	5.410745	-2.574633	8.642590
H	5.275605	-3.596927	8.328304
C	6.425024	-1.684067	8.403891
H	7.321936	-1.858695	7.830241
C	6.039120	-0.503971	9.075447
H	6.567059	0.434540	9.128673
N	2.030129	0.956505	9.013388
N	4.416881	2.147563	9.411418
N	5.428290	1.599457	11.739286
N	5.084516	0.316648	13.611876
N	4.024413	-0.237754	12.962486
N	2.596823	2.755330	11.803193
N	1.352905	0.359575	11.963467
N	2.604291	-1.526702	10.674420
N	4.486356	-1.925004	9.416284
N	4.871507	-0.648014	9.687027
Fe	3.388894	0.704336	10.905762